CHALMERS
UNIVERSITY OF TECHNOLOGY

Modelling of Generic Maximum Power Point Tracker for Wind Farms

Master's thesis in Electric Power Engineering

Joachim Andersson

Department of Energy and Environment
CHALMERS UNIVERSITY OF TECHNOLOGY
Gothenburg, Sweden 2015

Modelling of Generic Maximum Power Point Tracker for Wind Farms

Joachim Andersson

Department of Energy and Environment
Division of Electric Power Engineering
CHALMERS UNIVERSITY OF TECHNOLOGY
Göteborg, Sweden 2015

Modelling of Generic Maximum Power Point Tracker for Wind Farms

JOACHIM ANDERSSON

ISSN 1652-8557
Department of Energy and Environment
Division of Electric Power Engineering
Chalmers University of Technology
SE-412 96 Göteborg
Sweden
Telephone: +46 (0)31-775 1000

Cover:
Three Vestas V90 2 MW wind turbines outside Tvååker in Halland, Sweden.

Chalmers Reproservice
Göteborg, Sweden 2015

Modelling of Generic Maximum Power Point Tracker for Wind Farms

JOACHIM ANDERSSON
Department of Energy and Environment
Division of Electric Power Engineering
Chalmers University of Technology

Abstract

The emission of CO2 is a major problem in the world today due to the greenhouse effect. This is one of the reasons why wind power, as a renewable energy source, is increasing fast in the world today. An effective way of harnessing lots of wind power is to build large wind farms. However, the aero-dynamic interaction among wind turbines, called wake effect, makes control of wind farms complicated. In order to cope with this problem and maximize the production of wind farms, a so-called Maximum Power Point Tracker can be used.

This thesis develops and evaluates a Maximum Power Point Tracker algorithm based on optimization. As compared to the previous research in the topic, the algorithm in this thesis takes into account not only the wake effect but also the collector system losses. Moreover, it also considers reactive power dispatch, cable current capability and bus voltage limits. The evaluation shows that the active power output of a sample wind farm consisting of 18 wind turbines, rated 6 MW each, can increase by as much as 1.30 %. At the same time, the losses are decreased by up to 1 % as compared to only considering the wake effect. The corresponding increase by considering the wake effect only is 1.27 %. Finally, the algorithm is also implemented and verified in the power system analysis software DIgSILENT PowerFactory.

Keywords: Wind power, wind farm, wind farm controller, Maximum power point tracker, wind farm optimization

Acknowledgements

First and foremost, I would like to express my thanks and gratitude to my supervisor Jon Rasmussen at Solvina AB for his support and expertise throughout this Master thesis. Further thanks to Peiyuan Chen at Chalmers University of Technology who, apart from being my examiner, also provided me with useful insights and knowledge. Torbjörn Thiringer at Chalmers University of Technology deserves thanks for providing me with useful wind speed data. I would also like to thank Sven Granfors at Solvina AB for employing me. Last but not least, many thanks to the employees at Solvina AB for providing me with a nice working environment.

Joachim Andersson
Varberg, 2015-06-11

Nomenclature and abbreviations

Symbol	Quantity	Unit
v	Wind speed	$\mathrm{m/s}$
A	Rotor area	m^2
p	Pressure	Pa
ρ	Air density	$\mathrm{kg/m}^3$
a	Axial induction factor	-
F	Force	N
P	Active power	W
C_p	Power coefficient	-
C_T	Thrust coefficient	-
λ	Tip-speed ratio	-
β	Pitch angle	°
R_{rotor}	Rotor radius	m
D_{rotor}	Rotor diameter	m
v_{tip}	Blade tip speed	$\mathrm{m/s}$
ω	Turbine rotational speed	$\mathrm{rad/s}$
k	Wake decay constant	-
x	Turbine separation distance	m
R	Resistance	Ω
X_L	Inductive reactance	Ω
C	Capacitance	F
X_C	Capacitive reactance	Ω
Q	Reactive power	VAr
S	Apparent power	VA

Abbreviation	Explanation
PCC	Point of common coupling
TSO	Transmission system operator
MPPT	Maximum power point tracker
DFIG	Doubly-fed induction generator
SGFC	Synchronous generator full converter
KCL	Kirchhoff's current law
PEC	Power electronic converter
HVAC	High voltage alternating current
HVDC	High voltage direct current
SVC	Static var compensator
MPC	Model predictive control
ROCOF	Rate of change of frequency
LVRT	Low voltage ride through

Table of contents

1 Introduction

The emission of CO2 is a major problem in the world today due to the greenhouse effect. Fossil fuel based electricity generation, e.g. coal, gas and oil power, constitutes a large part of the emissions and consequently these sources of power has to be reduced or even replaced. Moreover, due to the Fukushima disaster, Germany has decided to decommission all nuclear plants in the country. All plants decommissioned need to be replaced since the energy demand is not decreasing but rather increasing. This is the reason why wind power, as a renewable energy source, is increasing fast in the world today.

1.1 Background

An effective way of harnessing lots of wind power is to build large wind farms. Such wind farms can consist of more than 100 wind turbines and are mostly located offshore due to better wind conditions which mean a more stable production [1]. As compared to a single wind turbine or a small group of wind turbines, these wind farms also come with an increased complexity, namely how to control the wind farm. A wind farm usually consists of a couple of radial lines with a number of connected wind turbines each. The radial lines are connected to a substation which in turn is connected to land, the so-called point of common coupling (PCC). It is desirable that the wind farm should behave as a conventional power plant as seen from PCC [2]. In order to do this, the wind farm controller may have several control actions. For example to decide how much power each wind turbine should deliver in order to meet the power demand from the transmission system operator (TSO) at PCC and to regulate reactive power exchange at PCC. A very important control goal is how each wind turbine in the wind farm should be controlled in order to maximize the total active power extracted by the wind farm. To do this, a so-called Maximum Power Point Tracker (MPPT) is used in the wind farm controller. Previous research on the subject has focused on maximizing the total wind farm output with respect to the wake effect, which basically means that the wind speed drops as it passes a wind turbine, without considering the loading of cables interconnecting the turbines [3] - [6]. This is closely connected to how reactive power production is dispatched in the wind farm. With the number of wind farms increasing in the power system, optimized control is becoming more and more important. There is thus a need for an accurate and generic MPPT model that optimizes active power production with respect to the wake effect while taking into account both reactive power production and cable capacity.

1.2 Aim

The aim of this thesis is to develop and evaluate a generic MPPT model, which takes into account collector system losses, reactive power dispatch and cable capacity, that can be used in load-flow and dynamical power system simulations. The model is to be implemented and verified in the power system analysis software DIgSILENT PowerFactory.

1.3 Tasks

In order to reach the aim of the thesis, the following main tasks can be defined:

1. Literature study
2. Development of MPPT model in Matlab/Simulink
3. Implementation and verification of the model in PowerFactory
4. Evaluation of the model

The main goal of the literature study is to give a firm knowledge base on wind power, wind farms and wind farm controllers in particular. This includes how a normal wind turbine works and how it is controlled in order to maximize its efficiency. Moreover, it is important to study how the actual wind affects and is affected by a wind turbine, the latter is referred to as wake effect. In order to develop a MPPT for a wind farm controller, it is essential to know how wind farms are designed in terms of topology, electrical connections etc. and also how existing wind farm controllers are designed.

The second part of the thesis is the actual development of the MPPT model for wind farm controllers that is to be used for load-flow and dynamical power system simulations. As stated in Section 1.1, wind farms in the future power system must be able to behave similar to a conventional power plant. The consequence of this is that a wind farm controller must be able to perform different control actions, such as:

1. Active power regulation
    a. Ramp rate control
    b. Primary frequency control
    c. Inertia response
2. Reactive power regulation and voltage control
3. Low voltage ride-through

The main objective of active power regulation is to dispatch active power references to the individual wind turbines in the wind farm based on an active power reference for the wind farm given by the TSO. This dispatch is made according to certain rules, e.g. proportionally depending on how much active power each turbine can provide or according to different optimization goals. One such optimization goal is to maximize the active power extracted by the wind farm. This has already been done, e.g. in [4] and [6]. Sub-control actions to active power regulation includes ramp rate control, i.e. control how fast the active power exchange is allowed to change, frequency response in terms of primary frequency control and inertia response. Reactive power regulation means that the wind farm controller should be able to control how and where reactive power is produced/consumed in the wind farm. This includes dispatching reactive power references among the individual wind turbines and possibly also to reactive power compensators located within the wind farm. How this is done depends on what strategy that is implemented. For example, power factor control mode means that the reactive power in the wind farm is regulated so that the power factor is kept constant at PCC. Another example is that the TSO sends a reactive power reference to the wind farm controller which, similar to active power regulation, dispatches reactive power references to the wind turbines

according to a proportional distribution. In previous research, reactive power dispatch has been performed decoupled from the active power optimization. Voltage control is basically another name for controlling the voltage at PCC. To add complexity, there is a second level of voltage control at each individual turbine. This voltage controller tries to keep the terminal voltage of that turbine within certain limits. Due to this, there is a limit to the amount of reactive power that can be demanded at PCC. LVRT means that a wind farm should be able to stay connected to the grid during a voltage dip according to the grid code requirement. This is an important criterion to fulfill in wind power dominated systems.

The MPPT to be developed in this thesis should, as compared to e.g. [4] and [6], also take into consideration how cable losses are affected as well as possible cable overloading due to reactive power. Moreover, it should also take into account how the optimized active power dispatch affects how reactive power is to be dispatched within the wind farm. The model should be generic in the sense that it can be used for wind turbines from different manufacturers and for wind farms with different layouts. It should also be able to handle a situation when one or more wind turbines are out of service.

In the third part of the thesis, the developed MPPT model is to be implemented in the power system analysis software PowerFactory. Moreover, the model has to be verified so that it works as intended. PowerFactory includes generic wind turbine models that will have to be slightly modified before they can be used in the thesis. The final part of the thesis is to evaluate the model's performance. To do this, a more complex power system than used for the verification process is preferable. The verification and evaluation will be done for both load-flow and dynamic simulations.

1.4 Scope

The dominating wind turbine configuration today is the variable speed, pitch-regulated turbine [2]. The electrical system of those turbines is mainly doubly-fed induction generator (DFIG) or a synchronous generator with full converter (SGFC). PowerFactory includes built-in wind turbine models for both DFIG and SGFC configurations. However, it is only the DFIG model that is detailed enough for this type of study. Due to this, only DFIG turbines will be used in the verification and evaluation process.

The main focus in the thesis is on developing, verifying and evaluating an MPPT for wind farm controllers. In order to do this, the wind experienced by the wind turbines in the wind farm does not have to be modelled in a very realistic manner. Instead, the incoming wind will be considered as constant or varying in a step-like manner. However, the wake effect will be considered since it has a significant impact on the active power production of a wind farm [3]. By considering the wake effect, each wind turbine in the wind farm will experience a wind speed that is determined by the wind farm topology, wind direction, the incoming wind speed as well as the operating point of each wind turbine. Since the number of combinations is infinite, only three extreme cases will be considered. First, the wind direction is orthogonal to the wind farm radials. Second, the wind direction is in line with the radials with the upwind wind turbine located at the substation. Third, the wind direction is also in line with the radials but the upwind wind turbine is located farthest away from the substation.

The topology of a wind farm, i.e. how the wind turbines are located within the wind farm and how they are electrically connected, is very important. It, for instance, influences the wake effect and collector system losses. Only one topology will be considered since it is enough for verifying and evaluating the MPPT model. Moreover, only High Voltage Alternating Current (HVAC) connected wind farms will be considered and not High Voltage Direct Current (HVDC) connections since HVAC is the most common system used today [7].

1.5 Contributions

Coordinated wind farm control has been a hot research topic within the field of wind energy during the last years. This has led to the development of several methods, with very different approaches, of how to maximize the active power output of a wind farm. For example in [3], the optimization problem is solved analytically for a simplified wake effect model. In [6], a model free approach, i.e. no wake effect model or wind turbine model is needed, is used where the gradient of the active power output of the wind farm is used to update the control signals of the individual turbines. A more complex control strategy based on model predictive control (MPC) is implemented in [4]. All of these methods have in common that it is only the production of all the wind turbines that is considered, not the actual output of the wind farm as a whole. Moreover, none of the methods takes the dispatch of reactive power into consideration. In this thesis, the optimization goal is to maximize the active power output of the wind farm. This implies that collector system losses are to be considered in the optimization, a consideration that has not been included in previous work on the topic. Moreover, the reactive power dispatch is also embedded into the optimization which provides a more realistic analysis.

1.6 Report structure

Chapter 2 covers fundamendal theory that is needed in order to understand the development of the MPPT. This includes a description of reactive power capability of wind turbines, some basic actuator theory, how wind turbines are operated to maximize efficiency etc. This chapter also gives a short review of offshore wind farms.

The next chapter, Chapter 3, describes the development of the MPPT including an explanation of the optimization procedure. This includes derivation of cost functions and constraints. Moreover, steady-state tests and Simulink simulations are made to evaluate the performance of the MPPT.

Chapter 4 describes how the MPPT developed in Chapter 3 is implemented in PowerFactory. An evaluation of the MPPT is made in Chapter 5 to ensure that it works as intended. The final chapters include discussion and conclusions.

2 Wind power in power systems

This chapter covers the basic knowledge about wind, wind turbines, wind farms and wind farm controllers that is needed to understand how the MPPT is developed in Chapter 3.

2.1 Reactive power capability of wind turbines

Both DFIG and SGFC wind turbines are equipped with power electronic converters (PEC) to achieve variable speed operation. One important feature of PEC is that they are able to control active and reactive power independently of the other. However, the reactive power capability of a wind turbine is highly dependent on the current operating point in terms of active power output and terminal voltage.

A DFIG wind turbine is based on an induction generator with the stator connected to the grid through a three-winding transformer. The rotor winding of the induction generator is connected to the three-winding transformer via a PEC. This set-up makes it possible to control the rotor currents which in turn make it possible to control the reactive power output from the stator. Moreover, reactive power can also be produced by the PEC itself but the main source is still the induction generator. Due to this, there are three quantities limiting the reactive power capability, namely the rotor voltage, the rotor current and the stator current [8]. Moreover, the rotor voltage limit is affected by the stator voltage, so indirectly the stator voltage is also affecting the reactive power capability. The actual capability is often given in form of a PQ-curve where the reactive power capability limits are plotted as a function of output power and stator voltage. A sample DFIG PQ-curve for three different stator voltages is shown in Figure 1. The negative reactive power limit of -0.44 p.u. is caused by the stator current limit and the positive reactive power limit of 0.44 p.u. is caused by the rotor current limit [8]. As can be seen, the reactive power capability is highly dependent on active power output as well as stator voltage.

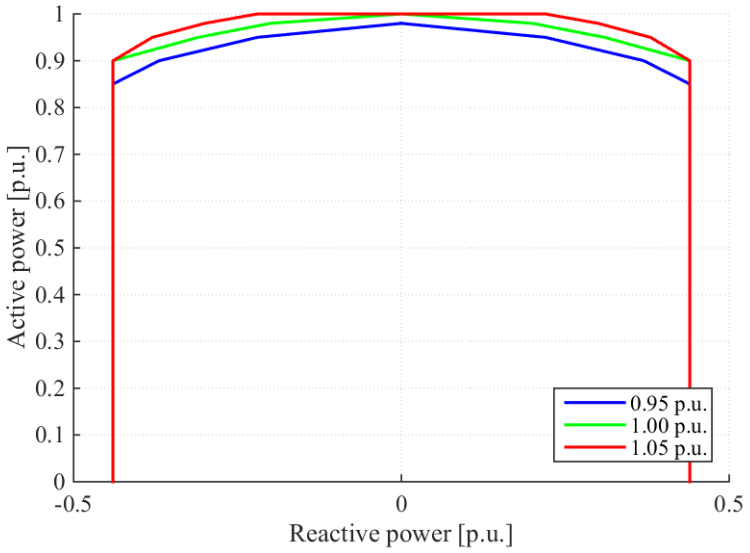

Figure 1: Sample PQ-curve of a DFIG wind turbine. Positive reactive power indicates injection into the grid.

In a SGFC wind turbine, the stator of the generator is connected to the grid via a PEC which gives full control of both active- and reactive power. In this set-up, all the reactive power is produced by the PEC which means that the reactive power capability is only limited by the current limit of the PEC. This limit is in turn related to the total apparent power output of the PEC, thus the reactive power capability can be expressed as

$$Q_{max} = \sqrt{S_{max}^2 - P_{actual}^2} \tag{1}$$

where S_{max} is the rated apparent power of the PEC in VA and P_{actual} is the current active power output of the PEC in W.

2.2 Actuator disc theory

The energy extraction performed by a wind turbine can be explained using the actuator disc concept. The wind turbine is replaced by an actuator disc which is simply a device that extracts energy from the wind that passes through it while it does not affect the wind that is not passing through it [1]. Consider the setup shown in Figure 2 where v represents wind speeds, A cross-sectional areas and p pressure. The indices ∞, D and W represents values for far upstream, at the disc and far downstream in the so-called wake. Throughout the whole system, the mass flow rate must be the same, i.e.

$$\rho A_\infty v_\infty = \rho A_D v_D = \rho A_W v_W \tag{2}$$

where ρ is the density of air. The disc causes a change in the wind speed that is given by

$$v_D = v_\infty(1 - a) \tag{3}$$

where a is the so-called axial induction factor [1]. The change in wind speed between far upstream and far downstream is $v_\infty - v_W$. This gives the following change in momentum

$$Change\ in\ momentum = (v_\infty - v_W)\rho A_D v_D \tag{4}$$

This change in momentum is caused by the pressure difference between upstream and downstream, i.e.

$$(p_D^+ - p_D^-)A_D = (v_\infty - v_W)\rho A_D v_\infty(1 - a) \tag{5}$$

From [1], the pressure difference is given by

$$(p_D^+ - p_D^-) = \frac{1}{2}\rho(v_\infty^2 - v_W^2) \tag{6}$$

Inserting (6) in (5) gives

$$\frac{1}{2}\rho(v_\infty^2 - v_W^2)A_D = (v_\infty - v_W)\rho A_D v_\infty(1 - a) \tag{7}$$

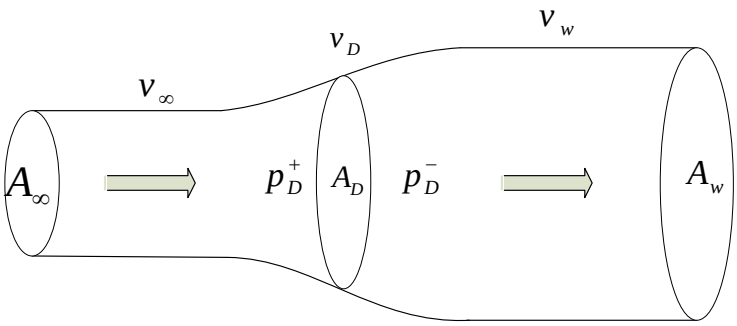

Figure 2: An actuator disc representing a wind turbine.

Solving (7) for v_w results in

$$v_W = v_\infty(1 - 2a) \tag{8}$$

By combining (5) and (8), the force experienced by the disc becomes

$$F = (p_D^+ - p_D^-)A_D = 2\rho A_D v_\infty^2 a(1 - a) \tag{9}$$

Finally, the power extracted by the disc can be calculated as

$$P = F \cdot v_D = \frac{1}{2}\rho A_D v_\infty^3 \cdot 4a(1 - a)^2 \tag{10}$$

Using the following definition of the so-called power coefficient

$$C_P = \frac{P}{\frac{1}{2}\rho A_D v_\infty^3} \tag{11}$$

it can be expressed as a function of the axial induction factor by combining (10) and (11) [1]. This gives

$$C_P = 4a(1 - a)^2 \tag{12}$$

which will be used in the MPPT development in Chapter 3. Moreover, by defining the so-called thrust coefficient as

$$C_T = \frac{F}{\frac{1}{2}\rho A_D v_\infty^2} \tag{13}$$

it can also be expressed as a function of the axial induction factor by combining (9) and (13) [1]. This gives

$$C_T = 4a(1 - a) \tag{14}$$

which will be used in the wake effect model in Section 2.4.2.

2.3 Operation of variable speed wind turbines

The power extracted from the wind by a wind turbine is given by the well-known formula

$$P = \frac{1}{2}\rho A C_p(\lambda, \beta) v^3 \tag{15}$$

where the power coefficient is a function of the blade pitch angle β and the tip-speed ratio λ, the latter is defined as

$$\lambda = \frac{v_{tip}}{v} = \frac{R_{rotor}\omega}{v} \tag{16}$$

where R is the rotor radius, ω is the turbine rotational speed. In order to extract as much energy as possible from the wind, the operational goal of a wind turbine is to maximize the power coefficient at all times. Hence, the control variables are turbine rotational speed and blade pitch angle. A typical $C_p(\lambda, \beta)$-curve for different pitch angles is shown in Figure 3. As seen, for each blade pitch angle there is a certain tip-speed ratio that maximizes the power coefficient.

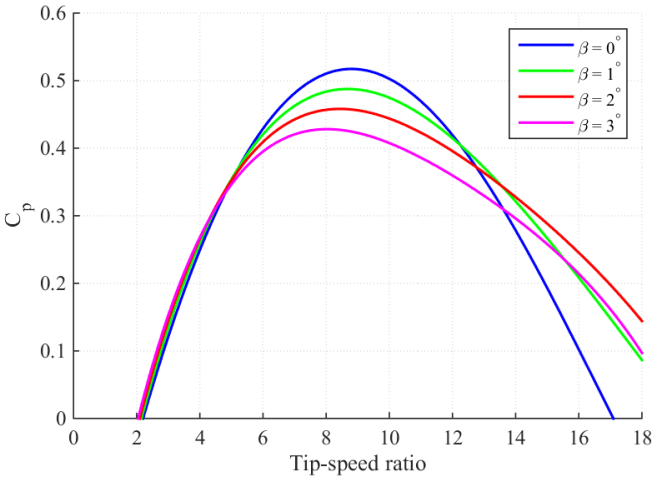

Figure 3: Typical power coefficient curve for four different pitch angles.

Due to electrical and mechanical design constraints this operation can be divided into three intervals, the low wind speed interval, the mid wind speed interval and the high wind speed interval. Figure 4 - Figure 6 shows example curves of optimal steady-state values of turbine speed, turbine power and pitch angle with the three intervals marked. In the low wind speed interval, which starts at the cut-in wind speed of the wind turbine, the blade pitch angle is fixed to its lowest value in order to extract as much power as possible from the wind. The control goal is therefore to adjust the turbine rotational speed in order to get the tip-speed ratio that maximizes the power coefficient. As the wind speed increases, the rotational turbine speed also increases. However, due to mechanical design constraints there is a maximum steady-state turbine speed limit. The wind speed at which this limit is reached defines the end of the low wind speed interval and the start of the mid wind speed interval, see Figure 4. At

this point, the rated power of the generator has not yet been reached so there is no need to increase the blade pitch angle. Instead, the new control goal is to maintain the maximum turbine speed limit as the wind speed increases. This control goal is valid up to the point when rated power of the generator is reached. At this point, the mid wind speed interval ends and the high wind speed interval starts, see Figure 5. In this interval, the control goal is to increase the blade pitch angle as the wind speed increases in order to limit the extracted power to the rated value of the generator while also maintaining the maximum turbine speed, see Figure 6.

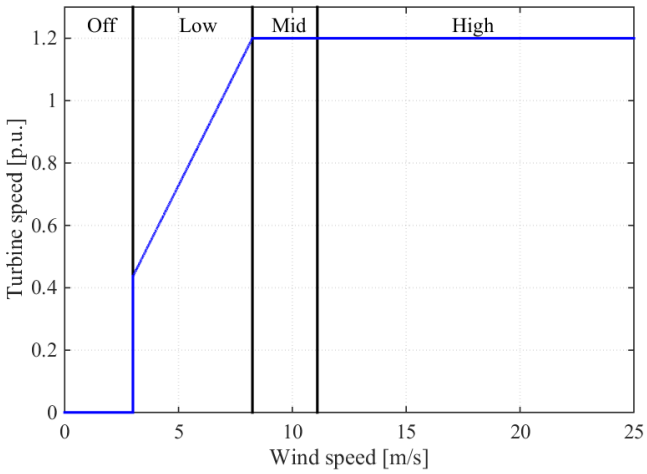

Figure 4: Optimal turbine speed at steady-state.

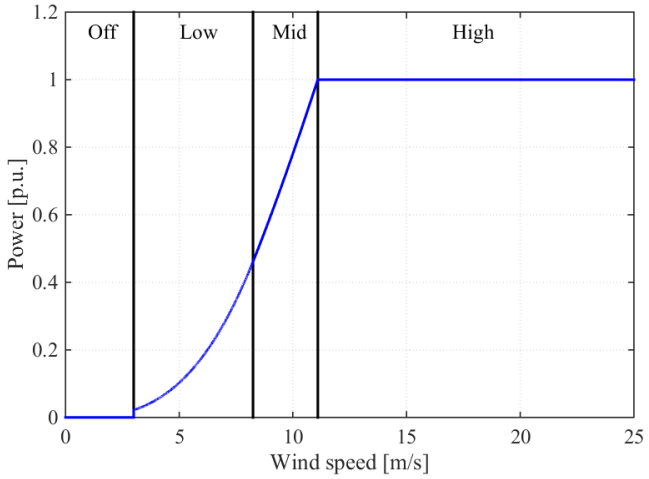

Figure 5: Optimal turbine power at steady-state.

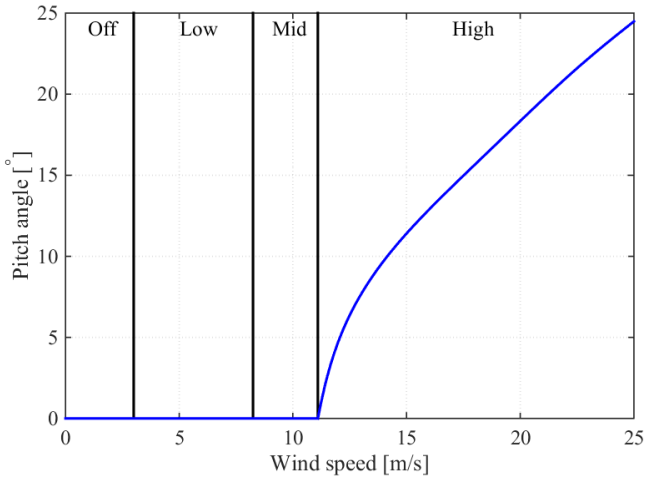

Figure 6: Optimal pitch angle at steady-state.

2.4 Offshore wind farms

Incitements for constructing large offshore wind farms are becoming stronger as the need for renewable power production is increasing. According to [1], important factors for this are for example:

- Huge areas available for construction
- High mean wind speeds
- Low wind turbulence
- Less visual impact

This section covers the features that characterize offshore wind farms and are considered important for the thesis, i.e. turbine micrositing, wake effect and electrical topology.

2.4.1 Wind turbine micrositing

How wind turbines are located with respect to each other inside a wind farm is called micrositing. This is very important since the wind turbines location with respect to each other greatly influences the performance of a wind farm. The reason for this is the aero-dynamical interaction between wind turbines, called the wake effect. Energy extracted by a wind turbine is taken from the kinetic energy in the wind. This leads to that the effective wind speed downstream a wind turbine is lower than the upstream wind speed. Due to the wake effect, it is essential that wind turbines are separated inside a wind farm. Typical separation distances are at least 5-6 rotor diameters in the wind direction for medium sized wind turbines [1]. Losses arising due to the wake effect can be considerable. As an example, Lillgrund offshore wind farm outside Malmö, Sweden, has comparably small separation distances leading to an overall wind farm efficiency of 77 % compared to without wake effect. This information was obtained from the Lillgrund Wind Farm, owned and operated by Vattenfall [9].

2.4.2 Wake effect model

A simple wake model is the so-called Park model which has been used frequently in the field of wind farm control during the last years [3], [5], [10]. The model is only valid in the far wake, i.e. far away from the upwind wind turbine, since it neglects the turbulence close downstream the wind turbine. According to [10], the Park model calculates the incident wind speed to wind turbine i as

$$v_i = v_\infty - \Delta v_i \tag{17}$$

where v_∞ is the free-stream, or incoming, wind speed and Δv_i is the wind speed deficit, i.e. the drop in wind speed. Assuming identical wind turbines, then the latter is given by

$$\Delta v_i = \sqrt{\sum_{k=1}^{i-1} \left(\delta v_{j,i}\right)^2} \tag{18}$$

in which

$$\delta v_{j,i} = v_\infty \cdot \left(1 - \sqrt{1 - C_{T,j}}\right) \cdot \left(\frac{D_{rotor}}{D_{rotor} + 2kx_{j,i}}\right)^2 \tag{19}$$

where $C_{T,j}$ is the thrust coefficient of wind turbine j, D_{rotor} is the wind turbine rotor diameter, k is the wake decay constant and $x_{j,i}$ is the distance between wind turbine j and wind turbine i. According to the Park model, the wake diameter increases linearly w.r.t. the distance $x_{j,i}$ as

$$D_{wake} = D_{rotor} + 2kx_{j,i} \tag{20}$$

Moreover, from (14) the factor $(1-\sqrt{1-C_{T,j}})$ is equal to $2a_j$ which gives the final wake effect model expression as

$$v_i = v_\infty - \sqrt{\sum_{j=1}^{i-1}\left(v_\infty \cdot 2a_j \cdot (\frac{D_{rotor}}{D_{rotor}+2kx_{j,i}})^2\right)^2} \tag{21}$$

2.4.3 Electrical system

An offshore wind farm can electrically be divided into two main parts, the collector system and the transmission system. The collector system connects all wind turbines to an offshore substation and can be built up using various topologies. The transmission system connects the offshore substation to a substation on shore. The latter uses either HVAC or HVDC for the connection in order to minimize losses. In this thesis, only HVAC is considered.

The electrical topology of the collector system defines how the individual turbines are electrically connected. Several topologies exist, both for AC and DC systems. The most common topology used for offshore applications is the AC radial connection as shown in Figure 7 [7]. Several cables, i.e. the radials, are connected to the substation. To each cable, several wind turbines are connected. To reduce costs, the radials can be built up with cables with decreasing cross-sectional area further away from the substation.

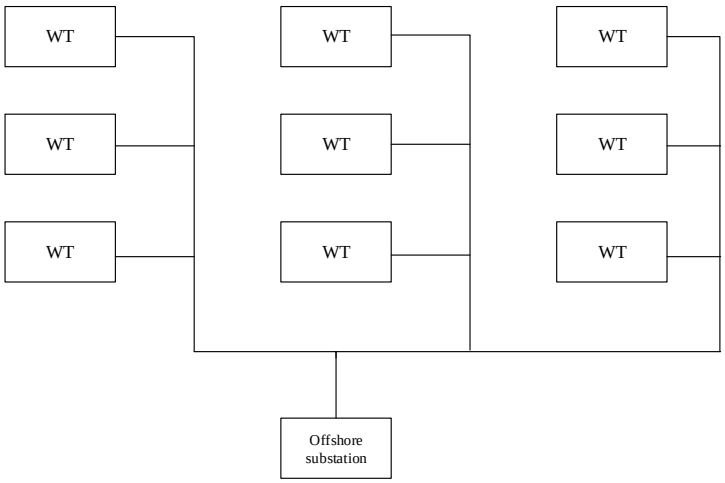

Figure 7: Radial connection topology for AC wind farms.

3 Development of Maximum Power Point Tracker model

This chapter covers development, testing and comparison of three different MPPT methods. The first method optimizes with respect to the wake effect and collector system losses, the second method optimizes with respect to the wake effect only and the third method is the conventional individual MPPT strategy where each wind turbine is controlled individually. The two latter methods are included in order to compare with the main method which is the wake effect and losses optimization.

3.1 Optimization algorithm

The MPPT design is to be formulated as an optimization problem and solved as such. Therefore some basic knowledge regarding optimization is needed and will be covered in this section together with the optimization itself. The basic optimization procedure is based on [11].

The first step in an optimization design process is to define the problem and its goals. This has already been done in Chapter 1 but is stated again here. The problem is how to coordinately control individual wind turbines in a wind farm in order to maximize the total active power output of the wind farm taking into account the wake effect as well as losses in the collector system. Moreover, the problem also includes how to dispatch reactive power references in order to fulfill the reactive power demand at PCC.

The second step is to gather information needed in order to solve the problem. In this particular problem, the information needed is the wake effect model and a collector system model including circuit parameters. The wake effect model is described in Section 2.4.2 and the collector system model in Section 3.3.1.

The third step is to identify the design variables. These variables are free in their nature and their values are chosen during the optimization process. This problem considers optimal control of wind turbines and it is thus natural to choose the wind turbine control variables as the design variables. Therefore, the design variables are chosen to be the power coefficients of the respective wind turbines, $C_{p,i}, \dots, C_{p,N}$ where N is the number of turbines in the wind farm. Moreover, the MPPT is supposed to also dispatch reactive power references to the wind turbines. To do this, the reactive power references of each turbine, $Q_{ref,i}, \dots, Q_{ref,N}$, will also be design variables.

The fourth step is to derive a so-called cost function that is to be minimized or maximized. The cost function is, directly or indirectly, a function of the design variables and returns a scalar value. In this problem, the cost function expresses the active power output of the wind farm as a function of the power coefficients and reactive power references of the wind turbines, i.e.

$$P_{farm} = f(C_{p,1}, C_{p,2} \dots C_{p,N}, Q_{ref,1}, Q_{ref,2}, \dots Q_{ref,N}) \tag{22}$$

The derivation of this expression is made in Section 3.1.1 and 3.1.2.

The fifth step is to identify possible constraints in the design. In this problem, the power coefficients are restricted to the interval $0 < C_{p,i} \leq C_{p,max}$ where $C_{p,max}$ is given by the actual turbine's power coefficient curve, see Section 2.3. The reactive power references are restricted to the interval $Q_{min,i} < Q_{ref,i} \leq Q_{max,i}$ where $Q_{min,i}$ and $Q_{max,i}$ are given by the PQ-curve of the actual wind turbine, see Section 2.1. Moreover, there are a number of functions that are implemented as nonlinear constraints. The calculations of these constraints are dependent on the result from the cost function and are therefore described in Section 3.1.3 to Section 3.1.7.

The final step in the optimization process is to minimize or maximize the cost function, in this case maximize, taking the constraints into consideration. This particular problem is a multivariable, nonlinear and constrained optimization problem. To solve such a problem numerical solvers are essential. The optimization problem in this thesis is solved using fmincon in Matlab which can handle multivariable, nonlinear and constrained optimization problems.

3.1.1 Cost function for wake effect optimization

When optimizing for the wake effect only, the goal is to maximize the total production of all the turbines in the wind farm by taking into account the aero-dynamic interaction among them. The cost function for such a problem formulation is the sum of the produced active power of all the turbines, expressed using the design variables as

$$P_{produced} = f(C_{p,1}, C_{p,2} \dots C_{p,N}) = P_1(C_{p,1}) + P_2(C_{p,2}, C_{p,1}) + \cdots + P_i(C_{p,N}, C_{p,N-1}, \dots, C_{p,1}) \quad (23)$$

where each turbine's power can be expressed as

$$P_i = \frac{1}{2}\rho A C_{p,i} v_i^3 \quad (24)$$

The wind speed that each turbine experiences can be expressed using the wake effect model described in Section 2.4.2 as

$$v_i = v_\infty - \sqrt{\sum_{j=1}^{i-1}\left(v_\infty \cdot 2a_j \cdot (\frac{D_{rotor}}{D_{rotor} + 2kx_{j,i}})^2\right)^2} \quad (25)$$

where the induction factors can be calculated from the power coefficients using (12). Using (25), the wind speed each turbine experiences can be expressed as a function of the incoming wind speed to the uppermost wind turbine and the induction factors. By combining (23), (24) and (25), the final cost function for the optimization is obtained. Since the closed-form expression becomes very long, it is not given here.

3.1.2 Cost function for wake effect, losses optimization

When considering wake effect and collector system losses, it is not the total active power production of all wind turbines in the wind farm that is of interest. Instead, it is the total active power output of the wind farm, i.e. the total active power production minus active power losses in the collector system, should be the cost function. Therefore, a load flow calculation has to be performed in order to find out the active power output.

Consider a bus in the collector system as shown in Figure 8. Applying Kirchhoff's current law (KCL) at the bus gives

$$\begin{aligned} I_i &= y_{i0}V_i + y_{i1}(V_i - V_1) + y_{i2}(V_i - V_2) + \cdots + y_{in}(V_i - V_n) \\ &= (y_{i0} + y_{i1} + y_{i2} + \cdots + y_{in}) - y_{i1}V_1 - y_{i2}V_2 - \cdots - y_{in}V_n \end{aligned} \tag{26}$$

where I_i is the current of bus i, $y_{i0} - y_{in}$ are the branch admittances connected to bus i and $V_1 - V_n$ are the bus voltages. Equation (26) can be rewritten as

$$I_i = V_i \sum_{j=0}^{n} y_{ij} - \sum_{j=1}^{n} y_{ij}V_j \quad j \neq i \tag{27}$$

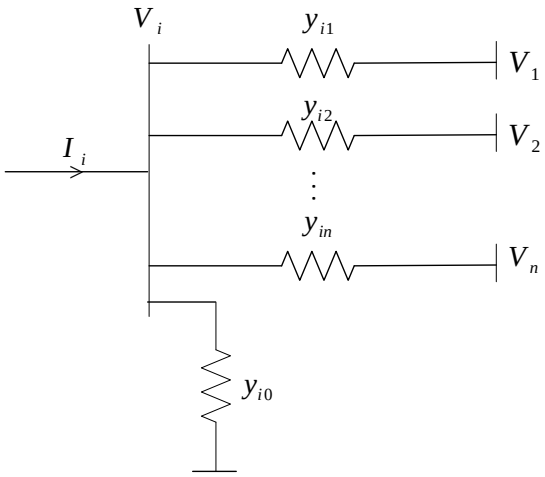

Figure 8: A generic bus in a power system.

For simplicity and ease of calculation, the branch admittances can be gathered in a matrix called the admittance matrix which has the following form

$$\boldsymbol{Y_{bus}} = \begin{bmatrix} Y_{11} & \cdots & Y_{1n} \\ \vdots & \ddots & \vdots \\ Y_{n1} & \cdots & Y_{nn} \end{bmatrix} \tag{28}$$

and where each element is defined as

$$Y_{ii} = \sum_{\substack{j=0 \\ \neq i}}^{n} y_{ij} \text{ and } Y_{ij} = -y_{ij} \text{ for } j \neq i \tag{29}$$

By using the admittance matrix, the current expression in (27) can be rewritten as

$$I_i = V_i Y_{ii} + \sum_{\substack{j=1 \\ \neq i}}^{n} Y_{ij} V_j = \sum_{j=1}^{n} Y_{ij} V_j \tag{30}$$

The current at bus i can also be expressed using the bus voltage and the active and reactive power at bus i according to

$$I_i = \frac{P_i - jQ_i}{V_i^*} \tag{31}$$

where P_i and Q_i is the active and reactive power at bus i and V_i^* is the complex conjugate of the voltage at bus i. Combining (30) and (31) gives

$$\frac{P_i - jQ_i}{V_i^*} = \sum_{j=1}^{n} Y_{ij} V_j \tag{32}$$

which is the so-called power flow equations that defines a system of nonlinear equations. Each bus has four quantities, $P, Q, |V|$ and δ where the latter is the bus voltage angle. For the system to be solvable, at least two quantities at each bus must be known. In a power system, three different kinds of buses can be defined, see Table 1. In this particular situation, PCC is modelled as a slack bus while each wind turbine is modelled as a PQ-bus. The system of nonlinear equations can be solved using different methods, for example Gauss-Seidel and Newton-Raphson. Due to the considerably faster convergence rate of the Newton-Raphson method, it is chosen to be used in this thesis.

Table 1: Bus types in a power system.

Bus type	Known	Unknown
Slack	$\|V\|, \delta$	P, Q
PV	$P, \|V\|$	Q, δ
PQ	P, Q	$\|V\|, \delta$

In the actual implementation as cost function in the optimization, a load flow program is needed to perform the calculation. Instead of writing a program from scratch, an already existing program, written by H. Saadat, is adopted [12]. The input to the load flow program is the active and reactive power of each turbine. The reactive power is a design variable so it is readily available. The active power is however not directly a design variable and it is calculated from the power coefficients, which are design variables. From (12), the induction factors can be calculated which can then be used to calculate the wind speed of each turbine using (21). With both wind speed and power coefficient known, the active power output of each turbine can be calculated using (24). The optimization procedure is summarized in the flowchart in Figure 9. Note that the flowchart is a simplified way of describing a complex procedure in the Matlab program fmincon performing the optimization.

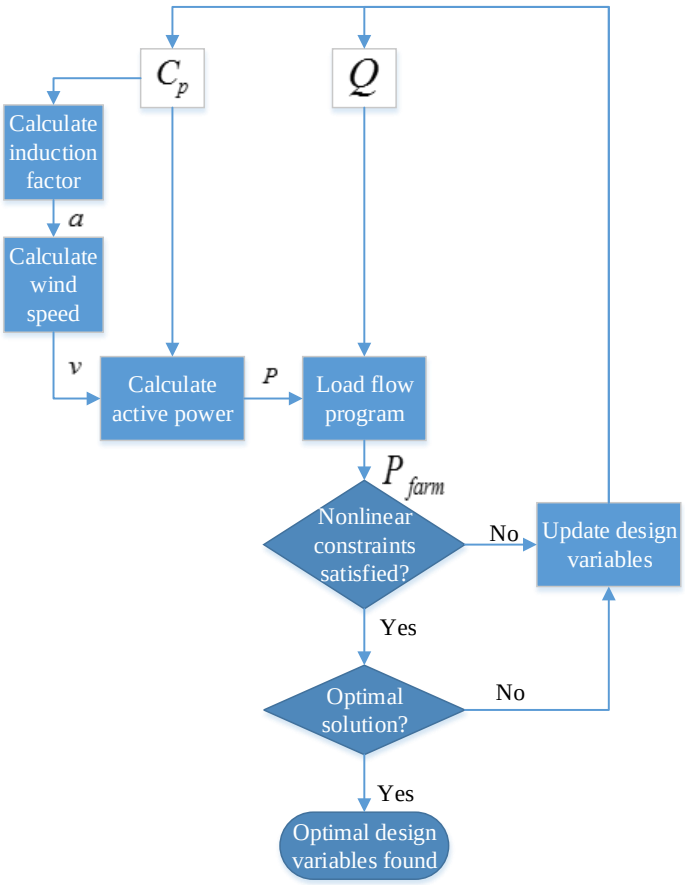

Figure 9: Flowchart of optimization procedure.

3.1.3 Cable capacity constraints

As is defined in Chapter 1, the rated current of the collector system cables must not be exceeded. This requirement is implemented as a nonlinear constraint. For each set of design variables, the non-linear constraint function calculates the current in each cable and compares it with the rated current, i.e.

$$I_i \leq I_{i,rated} \tag{33}$$

where I_i is the current in cable i and $I_{i,rated}$ is the rated current of cable i.

3.1.4 PQ-curve constraint

The concept of PQ-curve for a wind turbine is explained in Section 2.1. Since there is no point in sending reactive power references to the wind turbines that cannot be fulfilled due to the current operating state, the MPPT has a non-linear constraint which calculates the reactive power capability of each wind turbine at the current operating point using a PQ-curve. The references sent must then be within these limits, i.e.

$$Q_{i,min} \leq Q_{i,ref} \leq Q_{i,max} \tag{34}$$

where $Q_{i,ref}$ is the reactive power reference to turbine i and $Q_{i,min}$ and $Q_{i,max}$ are the minimum (inductive) and maximum (capacitive) reactive power limits of turbine i at the current operating point.

3.1.5 Bus voltage magnitude constraint

The bus voltage magnitude of each wind turbine must stay within certain limits from the nominal voltage. Therefore, the bus voltage magnitude has been added as a non-linear constraint according to

$$|V_{min}| \leq |V_i| \leq |V_{max}| \tag{35}$$

where $|V_i|$ the voltage magnitude of bus i, $|V_{min}|$ is the minimum allowable voltage magnitude and $|V_{max}|$ is the maximum allowable voltage magnitude. For each set of design variables, the bus voltage is calculated and compared to the above defined interval.

3.1.6 Turbine power constraint

In order to avoid sending active power references to the turbine that exceeds the rated power of the turbine a constraint is needed. This constraint simply checks that the active power output of each turbine is less than or equal to the turbine's rated power, i.e.

$$P_i \leq P_{i,rated} \tag{36}$$

where P_i is the actual active power output of turbine i and $P_{i,rated}$ is the rated power of turbine i.

3.1.7 Reactive power reference at PCC

The reactive power reference at PCC is implemented as a non-linear constraint where the actual reactive power output of the wind farm must be within a certain small interval around the reference, i.e.

$$0.99 \cdot Q_{farm,ref} \leq Q_{farm} \leq 1.01 \cdot Q_{farm,ref} \tag{37}$$

where $Q_{farm,ref}$ is the reactive power reference at PCC and Q_{farm} is the actual reactive power output of the wind farm. A small interval around the reference is chosen since it makes it easier to find a feasible solution as compared to an equality constraint, i.e. $Q_{farm} = Q_{farm,ref}$. The special case of $Q_{farm,ref} = 0$ MVAr is automatically replaced in the algorithm by $Q_{farm,ref} = 0.1$ MVAr using an if-statement. This has to be done in order to create an interval around the reference since one percent of zero is still zero. Since this non-linear constraint has to be fulfilled in order for the solver to converge to an optimal point, the reference cannot be outside the reactive power capability of the wind farm. This means that the reactive power capability has to be estimated prior to sending a reactive power reference. A script based on a while-loop with an embedded load-flow calculation of the whole wind farm is written to perform this task. The active power output of the wind turbines are kept constant to the values from the most recent MPPT update. The reactive power output of all turbines is then gradually increased/decreased at the same time in each lap in the loop until either maximum/minimum reactive power output of all turbines is reached or the upper/lower bus voltage limit of any bus in the system is reached. This script then outputs the maximum

(capacitive) and minimum (inductive) reactive power at PCC. Finally, the reactive power reference at PCC must be inside the interval defined by these two values. Note that since the active power output of each turbine is kept constant, the limits are a slight approximation.

3.2 MPPT update frequency

An important aspect to consider is the update frequency of the MPPT, i.e. how often the optimization algorithm is to be evaluated. Ideally, a high update frequency, i.e. to update often, is preferable since the optimal operating point of the wind farm can be traced better. However, since the optimization algorithm requires some time to be evaluated, the update frequency has an upper limit, i.e. an evaluation has to be finished before starting the next. Still, the update frequency cannot be too low, i.e. update seldom, since the MPPT must be able to track the varying wind speed as well as the reactive power demand at PCC.

In order to determine the update frequency requirement with respect to wind speed changes, wind speed data needs to be evaluated. Figure 10 shows measured wind speed data during a whole day for a wind turbine situated just outside the community of Tvåker in Halland, Sweden [13]. The wind speed data are averaged for 1 second and 15 minutes respectively. Figure 11 shows the wind speed variation probability within 15 minutes for the same set of data. The data are provided by prof. Torbjörn Thiringer at Chalmers University of Technology. The data indicate that the probability for a drastic change in the wind speed within 15 minutes is unlikely. As a consequence of this, the update frequency requirement with respect to changes in wind speed is low, to update once every other minute is reasonable.

The update frequency requirement with respect to reactive power is more complicated to determine depending on the requirements at PCC. For example, if the voltage magnitude is to be kept as constant as possible, i.e. voltage control, then the reactive power exchange from the wind farm has to be updated relatively fast. On the other hand, fine tuning (voltage control) is best implemented using a Static VAr Compensator (SVC) or STATCOM which provides fast and accurate reactive power exchange. In this thesis, voltage control is not considered as part of the MPPT objectives. Consequently, the reactive power references provided by the MPPT are for normal operating conditions only. Consider a situation where increased reactive power is needed instantly. A STATCOM in the wind farm would directly provide the needed reactive power. However, this depletes the reactive power reserve that the STATCOM provides. In order to restore the STATCOM reserve, the wind farm has to provide the extra reactive power needed and preferably as fast as possible. Therefore, the update frequency cannot be too low with respect to the reactive power.

The conclusion from above is that the update frequency requirement for both perspectives is comparably low even though the reactive power requires more frequent updates. As a trade-off between the two requirements, an update frequency of one update every 10 seconds is considered as an aim in this thesis.

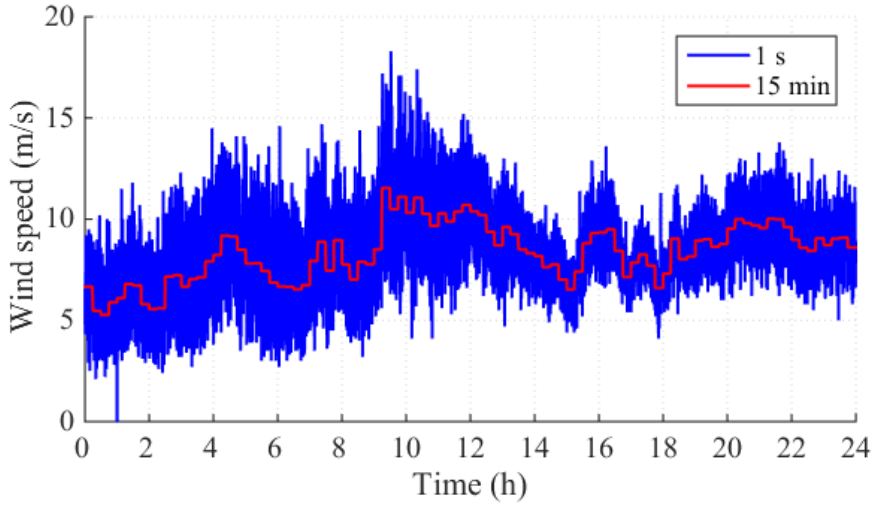

Figure 10: Measured wind speed data together with a 15 minute average.

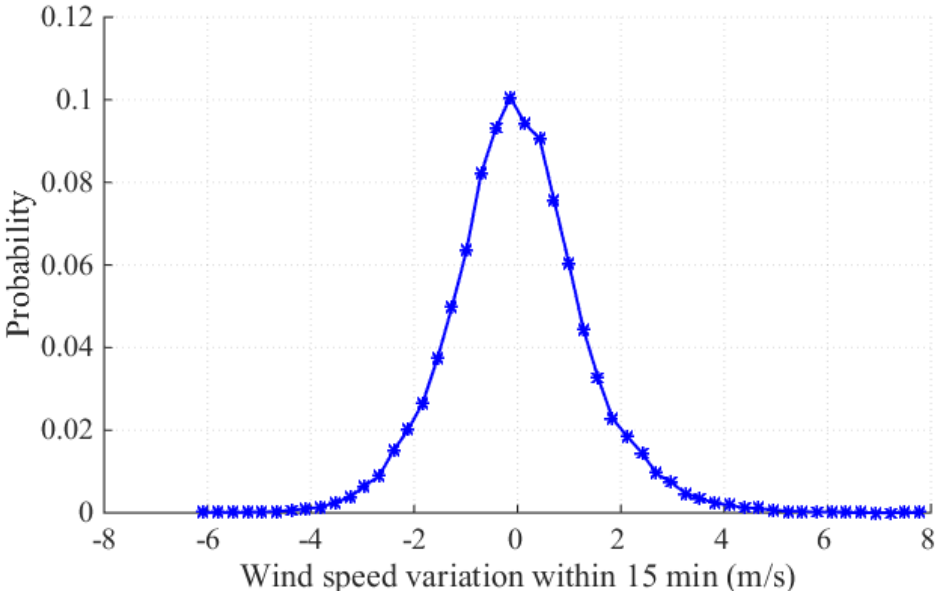

Figure 11: Wind speed variation probability for the wind speed data in Figure 10.

3.3 Steady-state tests and evaluation of optimization algorithms

In this section, steady-state tests and evaluation of the developed optimization algorithms are carried out in Matlab. Comparisons are made between individual MPPT operation, wake effect optimization and wake effect, losses optimization. In each test, three different wind directions are considered; orthogonal to radials and in line with radials with upstream wind turbine closest to substation and farthest away from substation respectively. In all tests, the incoming wind speed is 11 m/s.

One important part of the tests is to compare the results with different stopping conditions in fmincon. This is reflected in the solver tolerance, i.e. the difference between two consecutive cost function values. With higher tolerance, the computational time is reduced at the expense of less optimal result. One purpose of these tests is therefore to compare the result using different stopping conditions to see if the computational time can be reduced without reducing the accuracy too much. Therefore, three different tolerances are used ($10^{-2}, 10^{-4}$ and 10^{-6}) but the number of maximum iterations is kept fixed at 20000. This value is chosen since it leads to convergence for the optimization for all tolerances used in the thesis. Note that the time needed to perform 20000 iterations is affected by the computer used. Consequently, by using a faster computer the update frequency can be increased.

Three different tests are made with different reactive power output references. In the first test, the reference power output reference is 0 MVAr. In the second and third test, the reactive power output reference is put to maximum and minimum value respectively, as calculated by the method described in Section 3.1.7. Note that positive reactive power is defined as net export from the farm, i.e. capacitive operation, while negative reactive power is defined as net import to the farm, i.e. inductive operation.

The individual MPPT operation is implemented by manually setting the induction factor of each turbine to its maximum value. This ensures that the all turbines will capture as much energy as possible at all times. The reactive power output of each turbine is also set manually in order to fulfill the reference at PCC. This is done in the most intuitive way, i.e. to use the turbines closest to the substation first. If that is not enough to fulfill the reference, the second turbine on each radial is used and so on. The same constraints as for the two optimization algorithms is still used but checked manually so that no violation occurs.

3.3.1 Wind farm model used in the tests and simulations

A small wind farm is used in the simulations in this thesis. The wind farm consists of 18 wind turbines, rated 6 MW, sited in six rows and three columns and connected using an AC radial topology as shown in Figure 12. The separation distances between rows and between columns are both 1000 m. The cables connecting the turbines are of different cross-sectional areas with thicker cables closer to the substation in order to represent a real wind farm. The wake decay constant is set to 0.04 which is recommended for offshore applications [14]. Table 2 shows a summary of the parameter values used in the calculation.

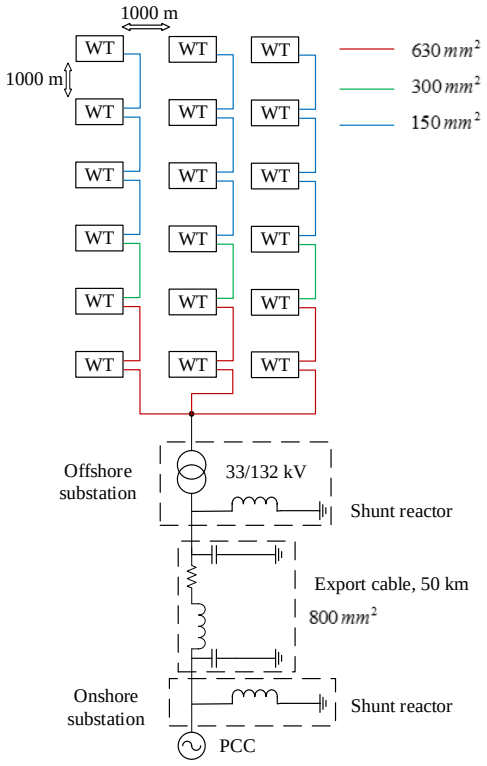

Figure 12: Layout of wind farm system used in the simulations.

Due to the capacitive behavior of cables, a suitable model to use is the π-model. Typical parameter values for the four different cable areas used in the wind farm are given in Table 3 [15]. With the transformer located in the nacelle the cable length is increased in both ends. Therefore, the length of each cable in the wind farm can be assumed to be a factor 1.15 longer than the separation distance. Rated voltage of the collector system and the export cable is 33 kV and 132 kV respectively. Static, inductive shunt compensators are connected at PCC and at the offshore substation in order to consume the reactive power produced by the export cable. The 33/132 kV step-up transformer in the offshore substation has static turns ratio.

Table 2: Parameter values used in the steady-state tests and comparisons.

Parameter	**Value**
Wake decay constant, k	0.04
Turbine separation, x	1000 m
Export cable length	50 km
Rotor diameter	154 m
Turbine rated power	6.0 MW at 11 m/s
Max power coefficient	0.5173 (a = 0.204)

Table 3: Cable model parameters used in the project simulations [15].

Area (mm^2)	R (Ω/km)	X_L (Ω/km)	C (μF/km)
800	0.058	0.114	0.224
630	0.065	0.110	0.350
300	0.105	0.120	0.265
150	0.180	0.130	0.208

3.3.2 0 MVAr reactive power demand at PCC

In this test, the reactive power demand at PCC is set to 0 MVAr. As described in 3.1.7, this reference is automatically replaced by 0.1 MVAr in the algorithm in order to create an interval in the non-linear constraint. The results from the test are shown in Table 4 - Table 6 for the three different wind directions. The results indicate that the two algorithms yield more or less the same active power output for all three wind directions. For the case shown in Table 5, the wake effect algorithm actually performs slightly better than the wake effect and losses algorithm. In case of orthogonal wind direction, the gain is very small, + 0.03 %, but for wind direction in line with the radials the gain is higher, +1.20 % and + 1.24 % respectively. When it comes to reactive power, all algorithms result in output at PCC within the $\pm$ 0.01 p.u. limit so it is acceptable. Concerning the computational time, the difference is not very big between the two optimization algorithms. Moreover, this test indicates that the result is not very dependent on the tolerances. The wake effect, losses algorithm performs equally good for all tolerances. The losses are higher for the two optimization algorithms than the individual MPPT strategy for all three wind directions. This is due to the increased active power output.

Table 4: Incoming wind direction orthogonal to radials, reactive power demand at PCC set to 0 MVAr.

Algorithm	**Wake effect and losses**			**Wake effect**			**Indiv. MPPT**
Tolerance	10^{-2}	10^{-4}	10^{-6}	10^{-2}	10^{-4}	10^{-6}	-
Active power (MW)	72.169	72.169	72.179	72.170	72.170	72.170	72.145
Comp. to ind. MPPT (%)	+0.03	+0.03	+0.03	+0.03	+0.03	+0.03	-
Losses (MW)	2.189	2.189	2.189	2.189	2.189	2.189	2.187
Reactive power (MVAr)	0.100	0.100	0.100	0.100	0.099	0.099	0.0300
Avg. reactive power per turbine	0.0188	0.0188	0.0188	0.0197	0.0197	0.0197	0.0267
Simulation time (s)	9.0	9.0	8.9	4.9	6.6	6.6	-

Table 5: Incoming wind direction in line with radials with upwind turbine closest to substation, reactive power demand at PCC set to 0 MVAr.

Algorithm	**Wake effect and losses**			**Wake effect**			**Indiv. MPPT**
Tolerance	10^{-2}	10^{-4}	10^{-6}	10^{-2}	10^{-4}	10^{-6}	-
Active power (MW)	62.486	62.486	62.486	61.487	62.487	62.487	61.749
Comp. w. ind. MPPT (%)	+1.20	+1.20	+1.20	+1.20	+1.20	+1.20	-
Losses (MW)	1.558	1.558	1.558	1.557	1.557	1.557	1.507
Reactive power (MVAr)	0.101	0.101	0.101	0.100	0.100	0.100	0.093
Avg. reactive power per turbine	-0.0646	-0.0646	-0.0646	-0.0536	-0.0536	-0.0536	-0.0600
Simulation time (s)	11.9	12.7	13.2	18.6	18.7	18.9	-

Table 6: Incoming wind in line with radials with upwind turbine farthest away from substation, reactive power demand at PCC set to 0 MVAr.

Algorithm	Wake effect and losses			Wake effect			Indiv. MPPT
Tolerance	10^{-2}	10^{-4}	10^{-6}	10^{-2}	10^{-4}	10^{-6}	-
Active power (MW)	62.383	62.383	62.383	62.385	62.385	62.385	61.618
Comp. w. ind. MPPT (%)	+1.24	+1.24	+1.24	+1.24	+1.24	+1.24	-
Losses (MW)	1.660	1.660	1.660	1.660	1.660	1.660	1.638
Reactive power (MVAr)	0.099	0.099	0.099	0.100	0.100	0.100	0.020
Avg. reactive power per turbine	-0.0595	-0.0595	-0.0595	-0.0485	-0.0485	-0.0485	-0.0600
Simulation time (s)	28.6	27.1	28.5	17.8	17.8	17.7	-

3.3.3 Maximum capacitive reactive power demand at PCC

The method described in Section 3.1.7 is used prior to this test in order to get an estimate of the maximum possible reactive power demand at PCC. This resulted in 12 MVAr for the orthogonal wind direction and 20.5 MVAr for wind direction in line with radials. This value is enforced by the bus voltage limits and not the reactive power capability of the wind turbines. Figure 13 shows the bus voltages in the wind farm for the data in Table 9. As can be seen, the bus voltage at the end of each radial is at its limit (1.05 p.u.). This means that the reactive power output cannot be increased more since that would violate the bus voltage non-linear constraint. If the bus voltage limits would have been changed to e.g. $\pm$ 0.1 p.u., there would have been more room to increase the reactive power output without violating the limits. Moreover, if the transformer would have been of tap-changing type it could have reduced the 33 kV side bus voltages in order to make room for more reactive power. The results are shown in Table 7 - Table 9 for the three different wind directions. This test indicates the same results as the test in Section 3.3.2, i.e. the difference between the wake effect, losses algorithm and the wake effect algorithm is small. Moreover, the tolerances does not influence the result very much and the computational time is similar between the algorithms. The results indicate that the wake effect and losses algorithm manages to increase the active power output by reducing the collector system losses, i.e. it finds a trade-off between the produced active power and the losses. This conclusion is based on the fact that the wake effect and losses algorithm performs better than the wake effect algorithm in all three cases while maintaining lower losses in the collector system.

Table 7: Incoming wind direction orthogonal to radials, reactive power demand at PCC set to 12 MVAr.

Algorithm	Wake effect and losses			Wake effect			Indiv. MPPT
Tolerance	10^{-2}	10^{-4}	10^{-6}	10^{-2}	10^{-4}	10^{-6}	-
Active power (MW)	72.148	72.148	72.148	72.141	72.143	72.143	72.121
Comp. w. ind. MPPT (%)	+0.04	+0.04	+0.04	+0.03	+0.03	+0.03	-
Losses (MW)	2.210	2.210	2.210	2.215	2.216	2.216	2.212
Reactive power (MVAr)	11.879	11.879	11.879	11.961	11.998	11.998	12.016
Avg. reactive power per turbine	0.6857	0.6857	0.6857	0.6905	0.6925	0.6925	0.6933
Simulation time (s)	19.3	18.3	18.5	2.9	10.5	10.6	-

Table 8: Incoming wind direction in line with radials with upwind turbine closest to substation, reactive power demand at PCC set to 20.5 MVAr.

Algorithm	**Wake effect and losses**			**Wake effect**			**Indiv. MPPT**
Tolerance	10^{-2}	10^{-4}	10^{-6}	10^{-2}	10^{-4}	10^{-6}	-
Active power (MW)	62.379	62.379	62.379	62.373	62.373	62.373	61.587
Comp. w. ind. MPPT (%)	+1.29	+1.29	+1.29	+1.28	+1.28	+1.28	-
Losses (MW)	1.665	1.665	1.665	1.672	1.672	1.672	1.670
Reactive power (MVAr)	20.295	20.295	20.295	20.295	20.295	20.295	20.373
Avg. reactive power per turbine	1.0795	1.0795	1.0795	1.0797	1.0797	1.0797	1.080
Simulation time (s)	22.6	22.0	21.4	32.2	32.3	32.3	-

Table 9: Incoming wind in line with radials with upwind turbine farthest away from substation, reactive power demand at PCC set to 20.5 MVAr.

Algorithm	**Wake effect and losses**			**Wake effect**			**Indiv. MPPT**
Tolerance	10^{-2}	10^{-4}	10^{-6}	10^{-2}	10^{-4}	10^{-6}	-
Active power (MW)	62.283	62.283	62.283	62.283	62.283	62.283	61.518
Comp. w. ind. MPPT (%)	+1.24	+1.24	+1.24	+1.24	+1.24	+1.24	-
Losses (MW)	1.758	1.758	1.758	1.766	1.766	1.766	1.739
Reactive power (MVAr)	20.308	20.308	20.308	20.418	20.418	20.418	20.486
Avg. reactive power per turbine	1.0846	1.0846	1.0846	1.0911	1.0911	1.0911	1.050
Simulation time (s)	14.9	16.7	15.2	22.4	22.3	22.2	-

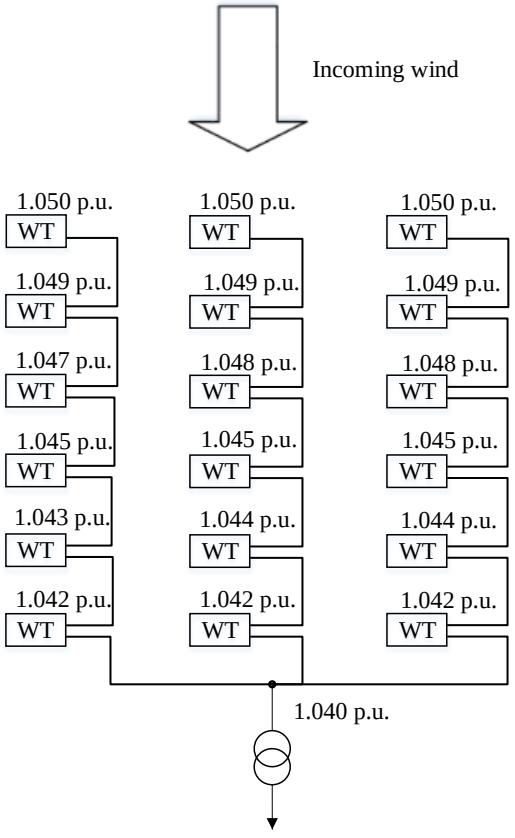

Figure 13: Bus voltages for the data in Table 9.

3.3.4 Maximum inductive reactive power demand at PCC

The method described in Section 3.1.7 is used prior to this test in order to get an estimate of the minimum possible reactive power demand at PCC. This resulted in -34 MVAr for the orthogonal wind direction and -40.5 MVAr for the wind directions in line with radials. The results are shown in Table 10 - Table 12 for the three different wind directions. In this test, the results indicate that the algorithm yielding the highest active power output from the wind farm is the wake effect, losses algorithm. The results are very similar to the capacitive case.

Table 10: Incoming wind direction orthogonal to radials, reactive power demand at PCC set to -34 MVAr.

Algorithm	**Wake effect and losses**			**Wake effect**			**Indiv. MPPT**
Tolerance	10^{-2}	10^{-4}	10^{-6}	10^{-2}	10^{-4}	10^{-6}	-
Active power (MW)	71.625	71.625	71.625	71.618	71.618	71.618	71.592
Comp. w. ind. MPPT (%)	+0.05	+0.05	+0.05	+0.04	+0.04	+0.04	-
Losses (MW)	2.710	2.710	2.710	2.739	2.740	2.740	2.741
Reactive power (MVAr)	-33.657	-33.657	-33.657	-33.672	-33.672	-33.672	-33.723
Avg. reactive power per turbine	-1.7583	-1.7583	-1.7583	-1.7573	-1.7573	-1.7573	-1.7600
Simulation time (s)	7.7	7.8	8.0	4.0	4.2	4.5	-

Table 11: Incoming wind direction in line with radials with upwind turbine closest to substation, reactive power demand at PCC set to -40.5 MVAr.

Algorithm	**Wake effect and losses**			**Wake effect**			**Indiv. MPPT**
Tolerance	10^{-2}	10^{-4}	10^{-6}	10^{-2}	10^{-4}	10^{-6}	-
Active power (MW)	61.753	61.753	61.753	61.739	61.739	61.739	60.982
Comp. w. ind. MPPT (%)	+1.26	+1.26	+1.26	+1.24	+1.24	+1.24	-
Losses (MW)	2.289	2.289	2.289	2.307	2.307	2.307	2.274
Reactive power (MVAr)	-40.095	-40.095	-40.095	-40.096	-40.096	-40.096	-40.630
Avg. reactive power per turbine	-2.1680	-2.1680	-2.1680	-2.1672	-2.1672	-2.1672	-2.200
Simulation time (s)	49.7	46.6	47.8	19.2	19.0	19.1	-

Table 12: Incoming wind in line with radials with upwind turbine farthest away from substation, reactive power demand at PCC set to -40.5 MVAr.

Algorithm	**Wake effect and losses**			**Wake effect**			**Indiv. MPPT**
Tolerance	10^{-2}	10^{-4}	10^{-6}	10^{-2}	10^{-4}	10^{-6}	-
Active power (MW)	61.690	61.690	61.690	61.671	61.671	61.671	60.900
Comp. w. ind. MPPT (%)	+1.30	+1.30	+1.30	+1.27	+1.27	+1.27	-
Losses (MW)	2.353	2.353	2.353	2.357	2.357	2.357	2.356
Reactive power (MVAr)	-40.076	-40.076	-40.086	-40.625	-40.625	-40.625	-40.697
Avg. reactive power per turbine	-2.1642	-2.1642	-2.1647	-2.1917	-2.1917	-2.1917	-2.200
Simulation time (s)	19.0	19.4	21.5	29.1	29.4	29.8	-

3.3.5 General conclusions from steady-state tests and comparisons

The wake effect, losses algorithm performs equally good as the wake effect algorithm except for the maximum inductive reactive power demand case in which it is slightly better. Moreover, the two algorithms are always better than the individual MPPT strategy. The improvement as compared to individual MPPT is up to 1.30 % which corresponds to 0.790 MW. The gain from considering losses on top of the wake effect is not very significant, about 0.01 % - 0.03 % which corresponds to 5 kW - 13 kW and can more or less be neglected as compared to the total wind farm output. In one case, the wake effect algorithm actually performs slightly better than the wake effect, losses algorithm. This is for the lowest losses case, i.e. when the reactive power demand reference is 0 MVAr. When the reactive power demand is either maximum capacitive or maximum inductive, the losses increases which causes the wake effect, losses algorithm to perform better than the wake effect algorithm. Consequently, the general conclusion is that with higher losses in the collector system, the wake effect, losses algorithm becomes more effective. This can be seen by comparing the losses between the cases for the different algorithms. In general, the losses are in the range 2-3 % of the wind farm output. By considering losses in the optimization, the total losses are decreased by 0.1 – 1 % as compared to only considering the wake effect. The biggest difference occurs when the reactive power output of the farm is at its limits, i.e. maximum capacitive/inductive. The downside of considering losses is that it in general takes longer time to perform the calculation. One important conclusion from these tests is that the computational time increases with lower tolerance. It will also increase with the number of wind turbines in the wind farm. It should be noted that the aim of performing a MPPT update every 10 seconds is not fulfilled in these tests. One way of fixing this issue is to increase the efficiency of the code, mainly by reducing the computational time of the load flow program. Moreover, tests on different computers have shown that the computer used greatly affects the computational time. In a real-life implementation the computer used will be specifically designed to handle the optimization which reduces the computational time further.

For the wind direction orthogonal to the radials, the gain from using the optimization algorithms as compared to the individual MPPT strategy is small. This is due to that there are only three turbines interacting with each other in that specific wind direction as compared to six turbines in the other wind directions. The more turbines in a row, the more prominent is the wake effect and it is therefore more beneficial to take the wake effect into consideration in the optimization. In case the wind farm would have consisted of six by six wind turbines, it is very likely that the two optimization algorithms would have performed considerably better than the individual MPPT strategy for all cases due to the stronger aero-dynamical interaction within the wind farm.

3.4 Dynamic tests of optimization algorithm

In order to test and evaluate the dynamic performance of the optimization algorithm, simulations are made in Simulink. The goal of these simulations is to test the following:

- Is steady-state reached?
- Can the algorithm handle wind speed steps?
- Can the algorithm handle reactive power reference steps?

Whether steady-state is reached after a change in the system is tested as a part of the two other tests, i.e. is steady-state reached after both a wind speed step and a reactive power reference step. The tests are only made for the wake effect, losses algorithm.

3.4.1 Simulink model

Since the main purpose of the simulations in Simulink is to test the dynamic performance of the optimization algorithm there is no need to model a big wind farm. Instead, to limit complexity and computational time of the model, only six turbines situated in one radial is considered. The incoming wind is in line with the radials with the upwind turbine farthest away from the substation.

The Simulink model, shown in Figure 14, consists of the six wind turbine blocks, a collector system block, a wake effect block and the MPPT block. The wind turbine used is the General Electric 2.5-103 Full Power Converter, since it is readily available to the author, modeled based on the work done in [16]. Important parameters for the wind turbine are given in Table 13. The model has been slightly modified in order for it to accept active and reactive power references as inputs. Each wind turbine block contains one wind turbine model. The collector system block contains a script which performs a load-flow calculation at each simulation step based on the produced active and reactive power of the wind turbines. The calculated bus voltages are sent back to the turbines where it is used to calculate the reactive power limits. The wake effect block determines the wind speed of each turbine, using the Park model, based on the incoming wind speed and the power coefficients of each turbine. The wake effect block also includes delays to model that it takes time for the wind to travel between turbines in the farm. The MPPT block includes the algorithm as described in the previous sections. Its inputs are incoming wind speed and farm reactive power reference. Outputs are active and reactive power references to the individual turbines.

Table 13: Parameters for General Electric 2.5-103 FPC wind turbine [17].

Parameter	Value
Rotor radius	56.6 m
Turbine constant $(0.5\rho A^2)$	3975
Rated active power	2.5 MW at 11 m/s
Rated apparent power	3.0 MVA
Max power coefficient	0.5173 (a = 0.204)

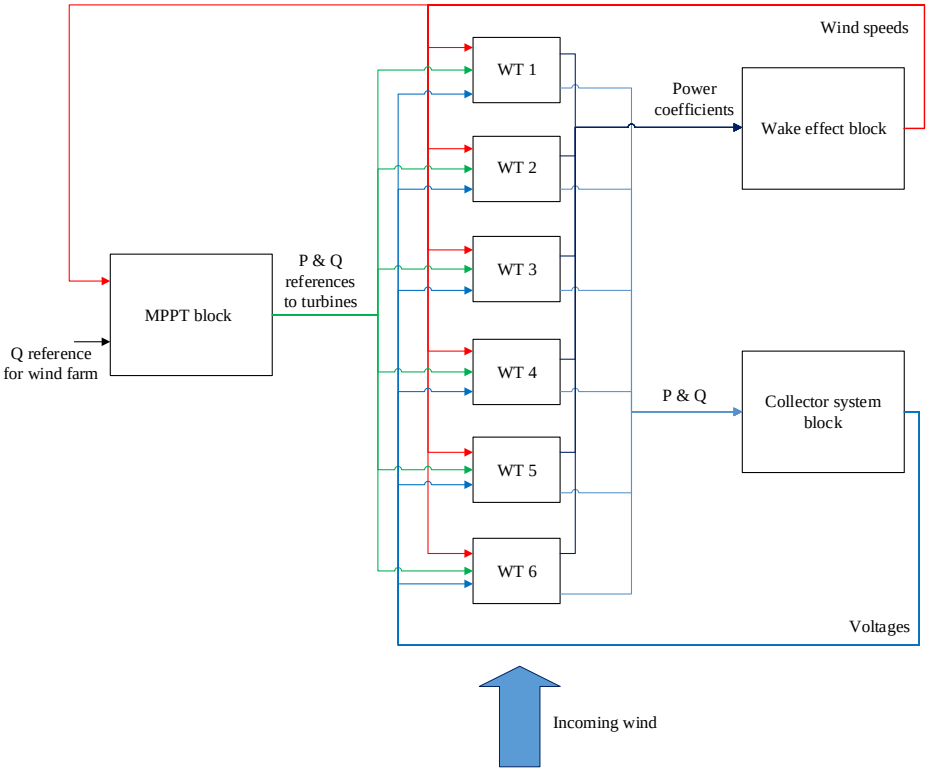

Figure 14: Block diagram of the Simulink model used.

3.4.2 Wind speed step test

In this test, the initial wind speed to the upwind turbine is 7 m/s. At $t = 5$ s, a wind speed step of 1 m/s occurs. The reactive power reference is kept constant at 0 MVAr throughout the whole simulation. The results from the simulation are shown in Figure 15 - Figure 20. Figure 15 shows the wind speed of each turbine.

At $t = 5$ s, the wind step occurs which changes the wind speed of the first turbine. Due to the travelling time between turbines it takes time for the step to propagate throughout the wind farm. At around $t = 850$ s, a new steady-state is reached since the wind has had time to propagate throughout the farm. The MPPT is only updated every 10 s, with start at $t = 0$ s, so the first update after the wind speed step is at $t = 10$ s. Since the MPPT is configured to update the active power references of all turbines based on the incoming wind speed of the first wind turbine, the first update at $t = 10$ s will result in new active power references to all wind turbines, without any delays, as can be seen in Figure 16. Figure 17 shows the turbine speed references that are calculated from the active power references and the incoming wind. This means that when the active power references change due to the MPPT update, the turbine speed references will also change as shown in Figure 17. Moreover, when the wind speed of an individual turbine changes the turbine speed reference of that turbine also changes which can be seen in Figure 17. The change in turbine speed causes the power coefficient to change which through the wake effect directly affects the wind speed behind each turbine. This explains the small overshoots of each wind speed step seen in Figure 15. The overshoots in the wind speed causes the turbine speed oscillations seen in Figure 18. Moreover, due to

the new and higher power references sent at $t = 10$ s every turbine will increase its active power output slightly even if the wind speed step has not arrived yet, see Figure 16. This increase in active power causes a change in operating point and which causes the wind speed to drop behind the turbines. The wind speed drop can be seen in Figure 15, just after the wind speed step reaches WT 5. In order to keep the turbine speed, shown in Figure 18, equal to the reference speed the electrical torque is adjusted as Figure 19 indicates. This explains the oscillations seen in the output active power of the wind farm in Figure 20. The low output power in the beginning of the simulation occurs when the MPPT has dispatched new active power references to the turbines. These new active power references in combination with the current wind speed results in higher turbine speed references than previously. To reach the new speed references, the turbine must accelerate which it does by reducing the electrical torque. Since all the turbines perform this control action at the same time, the total output active power of the wind farm is reduced considerably during this transient period. The only exception is WT 6 which increases its electrical torque in order to limit the turbine speed increase since it has already experienced the wind speed step.

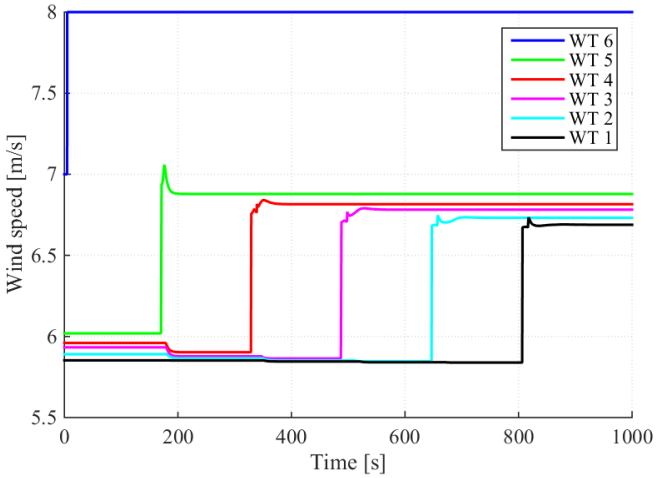

Figure 15: Wind speed of individual turbines.

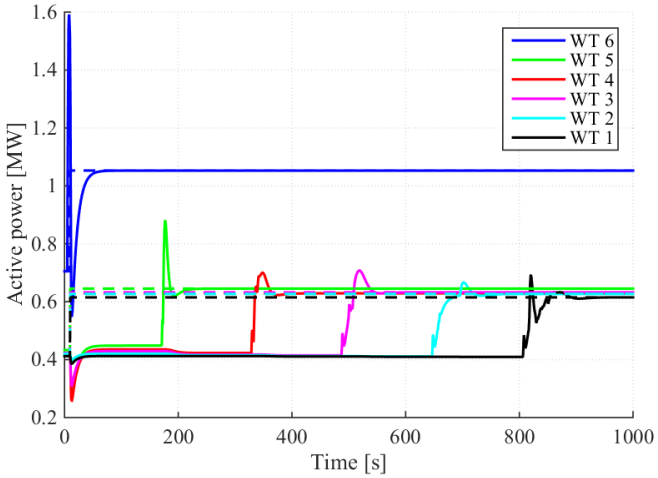

Figure 16: Active power and active power references of individual turbines, the dashed lines indicate the references.

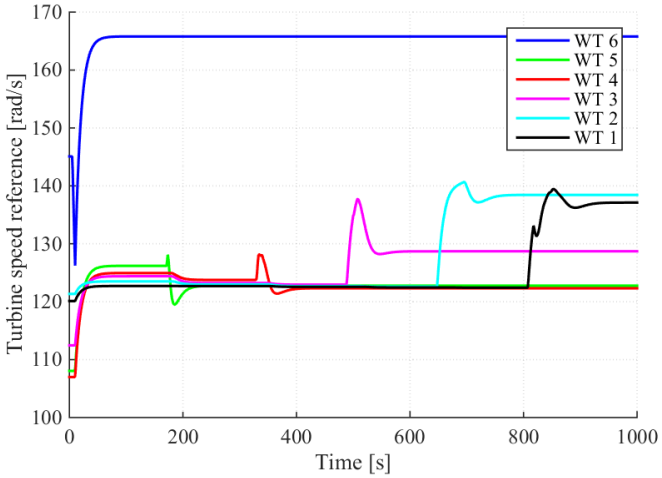

Figure 17: Turbine speed references of individual turbines.

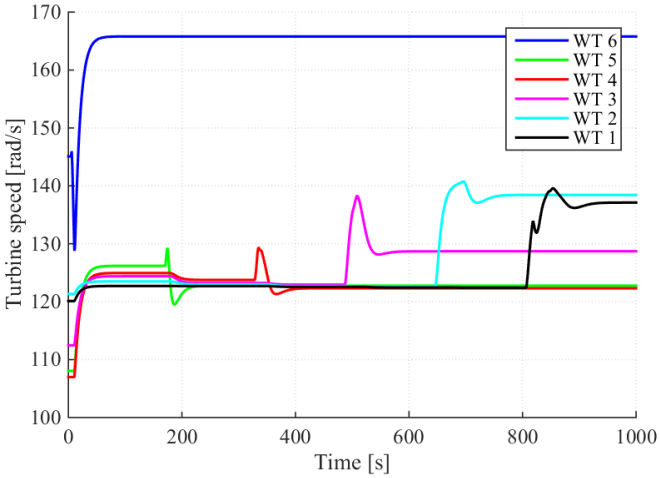

Figure 18: Turbine speed of individual turbines.

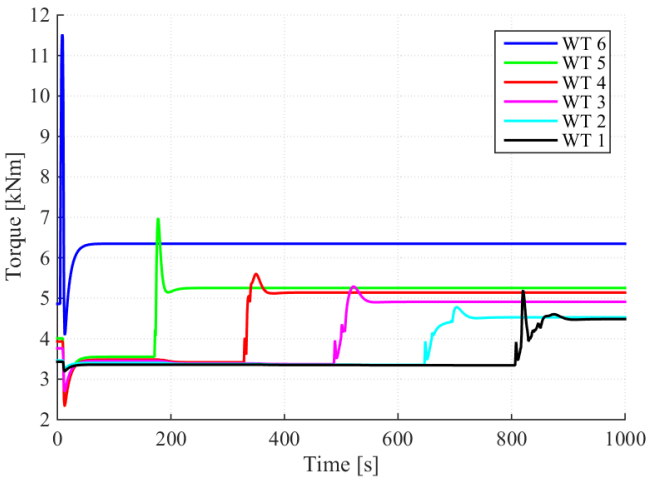

Figure 19: Electrical torque of individual turbines.

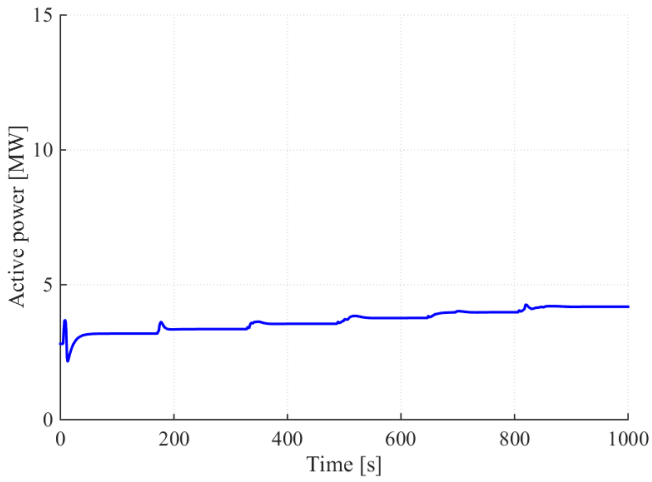

Figure 20: Active power output of wind farm.

3.4.3 Reactive power reference step test

In this test, the wind speed is $7\ \mathrm{m/s}$ and remains constant throughout the simulation. However, the reactive power reference, which is initially put to 0 MVAr, is stepped to 2.5 MVAr at $t = 5$ s. The results from the simulation are shown in Figure 21 - Figure 26.

Since the MPPT is only updated every ten seconds, the output changes at $t = 10$ s when the update takes place which can be seen in Figure 21. The reactive power output is not equal to the reference but within the tolerance as implemented in the optimization non-linear constraints. Due to that the reactive power demand has changed, the previous optimal solution is not valid any longer. This can be noticed in Figure 22 since the updated active power references differ from the old ones, i.e. a new optimization has been made for the new situation with updated reactive power reference and it resulted in different active power references. Since the turbine speed references are calculated from the active power references, the turbine speed references in Figure 23 changes, leading to a change in the electrical torque, Figure 25, in order for the turbine speeds in Figure 24 to reach the new reference speeds. The electrical torque of turbine 1, 2 and 4 is increased while the electrical torque of turbine 3 and 5 is decreased. The electrical torque of turbine 6 remains unchanged. The change in electrical torque is reflected in the output power increase just after $t = 10$ s, shown in Figure 26. The results indicate that the MPPT works as it should concerning reactive power reference changes.

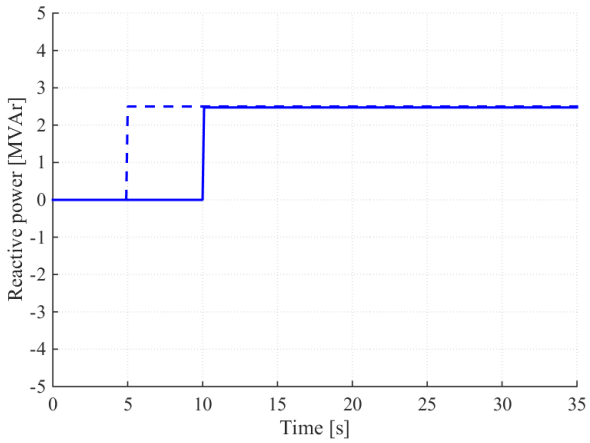

Figure 21: Reactive power output of wind farm, the dashed line is the reference.

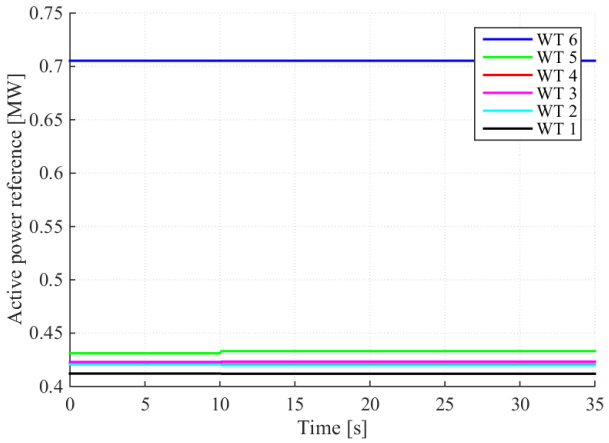

Figure 22: Active power references of individual turbines.

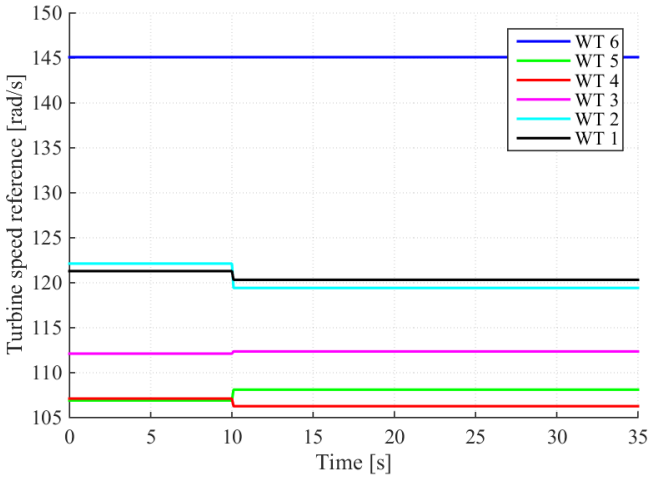

Figure 23: Turbine speed references of individual turbines.

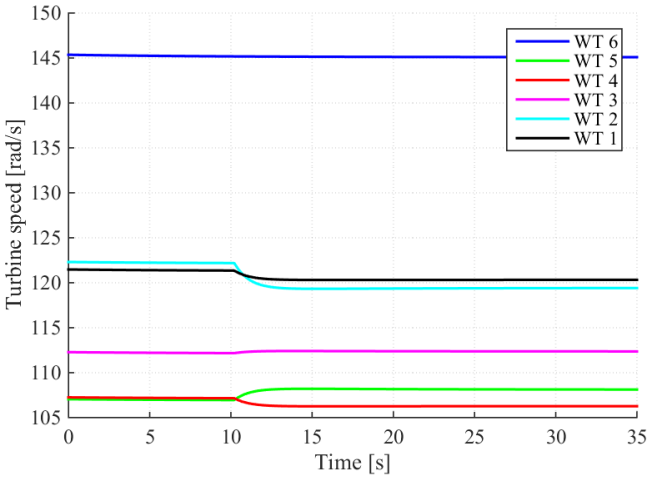

Figure 24: Turbine speed of individual turbines.

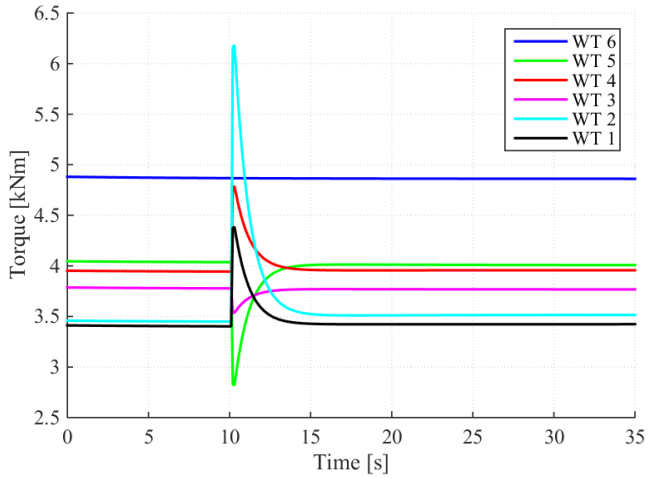

Figure 25: Electrical torque of individual turbines.

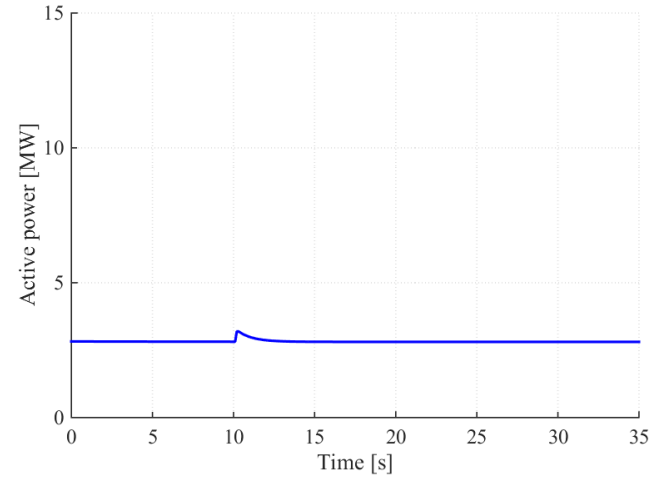

Figure 26: Active power output of wind farm.

4 Implementation in DIgSILENT PowerFactory

This chapter describes how the MPPT is implemented in PowerFactory. This includes a description of the modifications made to the existing wind turbine models in the software, how the wake effect is implemented and how the wind speed data is sent to each turbine. Moreover, the chapter covers how the MPPT is implemented via the Matlab interface that is built-in in PowerFactory.

4.1 DIgSILENT PowerFactory modelling approach

A model for dynamic simulations in PowerFactory is basically made up of two parts which are exchanging signals with each other. The first part is the grid containing various elements such as generators, transformers, transmission lines, loads, etc. The second part is the dynamic models of controllers, prime movers, turbines etc. Communication between the dynamic models and the grid elements is defined in a so-called frame, which is basically an overview diagram showing the signal routes. To build the grid of the wind farm described in Section 3.3.1 is straightforward. However, the dynamic model is more complicated and is therefore described in Section 4.1.1.

4.1.1 Dynamic Model in DIgSILENT PowerFactory

The dynamic model in PowerFactory, shown as a principal layout in Figure 27, consists of a frame with several slots which contain the MPPT, an incoming wind speed block, the wind turbines and several wake models. The MPPT slot contains an interface between PowerFactory and Matlab in which the actual optimization is performed, see Section 4.3 for further explanation. The incoming wind speed block simply contains a constant which represents the incoming wind speed to the farm. This constant can be changed during a simulation to represent e.g. a wind speed step. Each of the turbine slots contains a modified version of the built-in DFIG wind turbine control model, see Section 4.2 for further explanation on the modifications made. The wake model had to be split up into smaller models in between the turbines in order to be able to initialize the model correctly, see Section 4.4 for further explanation.

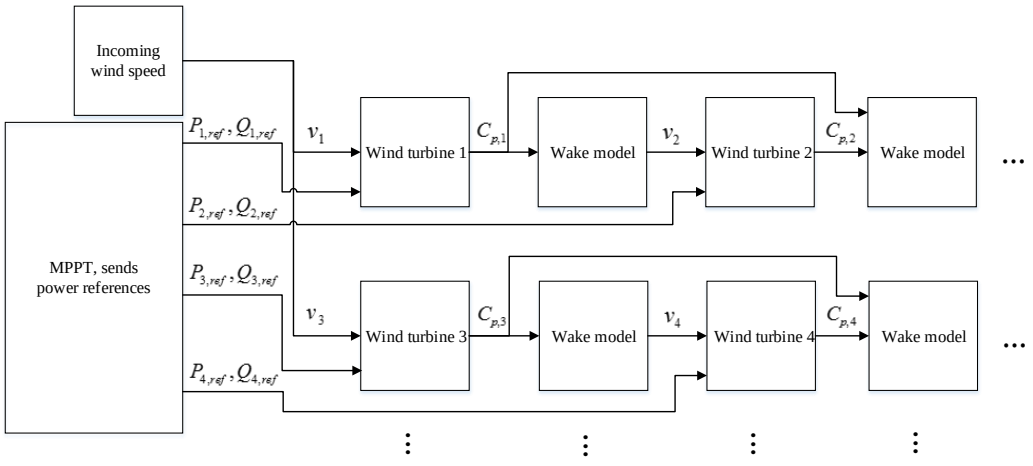

Figure 27: Principal layout of the dynamic model in PowerFactory, it can be extended as indicated by the dots.

4.2 Modification of wind turbine models

The built-in DFIG wind turbine models were originally created for grid integration studies and LVRT tests. Because of this, the models are not adapted to being controlled by a wind farm controller nor having a varying wind speed as input. However, in order to implement the MPPT designed in this thesis the DFIG wind turbine models must be able to be controlled by a wind farm controller, i.e. follow active- and reactive power references, and accept varying wind speed as input. Figure 28 shows a simplified block diagram of the modified DFIG wind turbine model, parts marked in red have been added or modified. In addition to the blocks shown in Figure 28 there is also a protection system that detects low terminal voltage and over/under frequency. In the case that the protection system detects e.g. low terminal voltage, countermeasures are taken, e.g. increase the reactive power output in case of low terminal voltage. This is added on top of the original power references in the PQ-controller.

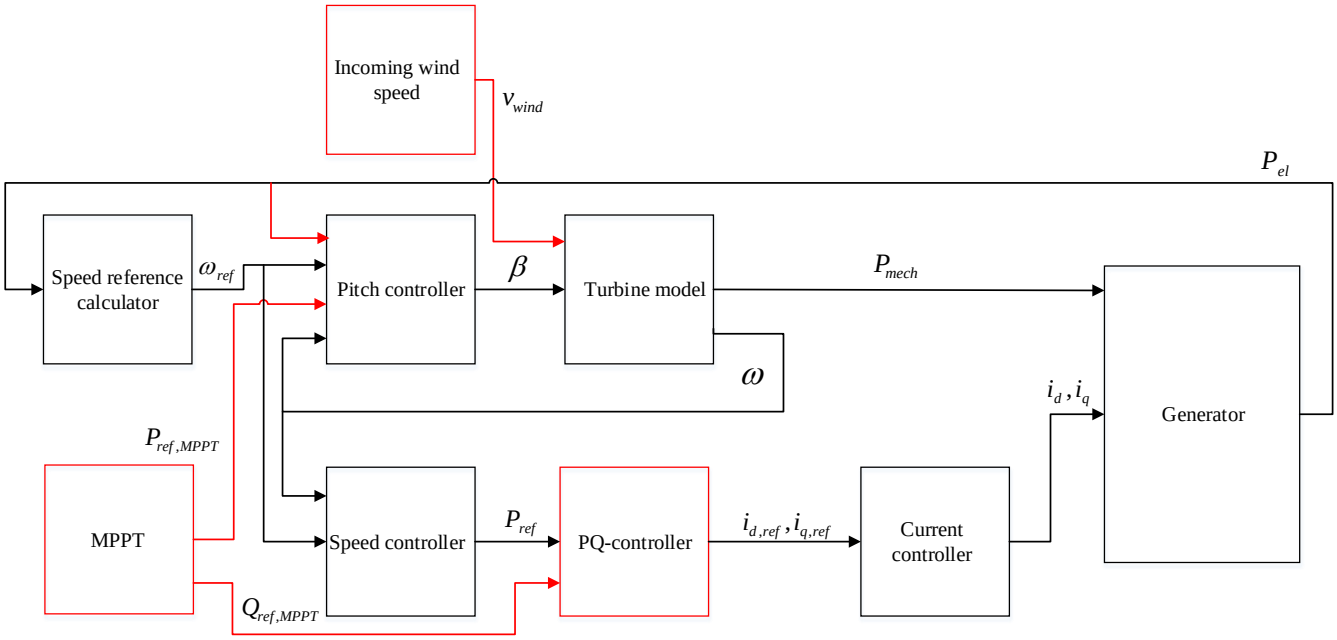

Figure 28: Simplified block diagram of the modified DFIG wind turbine model, parts marked in red have been added or modified.

4.2.1 Reactive power control

The built-in DFIG controller model in PowerFactory has a PQ-controller which has active- and reactive power references as inputs and rotor current references as outputs, see Figure 28. The reactive power reference is originally fixed to its initial value and only changes if the protection system is activated. However, since the MPPT sends reactive power references the DFIG controller must be able to accept and fulfill these. To do this, a new input is added to the PQ-controller connected directly to the reactive power reference output of the MPPT.

4.2.2 Wind speed input

Normally, the built-in DFIG controller model in PowerFactory uses a constant wind speed which is calculated based on the operating point at initialization, i.e. the active power output from the generator which is set before running the load-flow simulation. For implementing the MPPT, the wind turbine controller model must be able to have a wind speed input which is allowed to vary throughout the simulation. A new input is created, see Figure 28, and the initialization procedure is changed to allow an external wind speed.

4.2.3 Derated operation

The original DFIG wind turbine controller model is only able to operate at its individual maximum power point, i.e. it is capable of individual MPPT. When testing the MPPT designed in this thesis, the model must also be able to follow an active power reference, sent to it by the MPPT, which is lower than the maximum power point of the particular wind turbine. This is called derated operation and is performed by controlling the wind turbine to a power coefficient value that is lower than the optimal at the particular wind conditions. Three different methods can be used to achieve this; underspeeding, overspeeding and pitching. Over/underspeeding basically means that the turbine speed is adjusted so that the tip-speed ratio deviates from its optimal value. This leads to a lower power coefficient and thus lower mechanical input power to the wind turbine, see Figure 3. Derating by pitching is more straightforward since it uses the blade pitch angle to reduce the power coefficient. However, by using pitching for derated operation the mechanical wear in the pitching mechanism is increased. It might therefore be preferable from a practical point of view to use over/underspeeding which is performed using the PEC.

In this thesis, derated operation is done by pitching since it is easier to implement and the mechanical wear is not taken into account. An additional PI-regulator is added in the pitch controller, see the red dashed box in Figure 29. The input to this regulator is the difference between the actual active power output of the generator and the active power reference sent by the MPPT. The output of the PI-regulator is added to the existing pitch angle reference of the pitch controller. The added PI-regulator will ensure that the active power reference from the MPPT is fulfilled by adjusting the pitch which implies that derated operation is possible. Due to practical reasons, the pitch angle is limited to the interval between β_{min} and β_{max} . This is shown in the pitch actuator model, green dashed box in Figure 29, where the integrator can become saturated. To avoid integrator windup caused by the saturation, anti-windup is implemented.

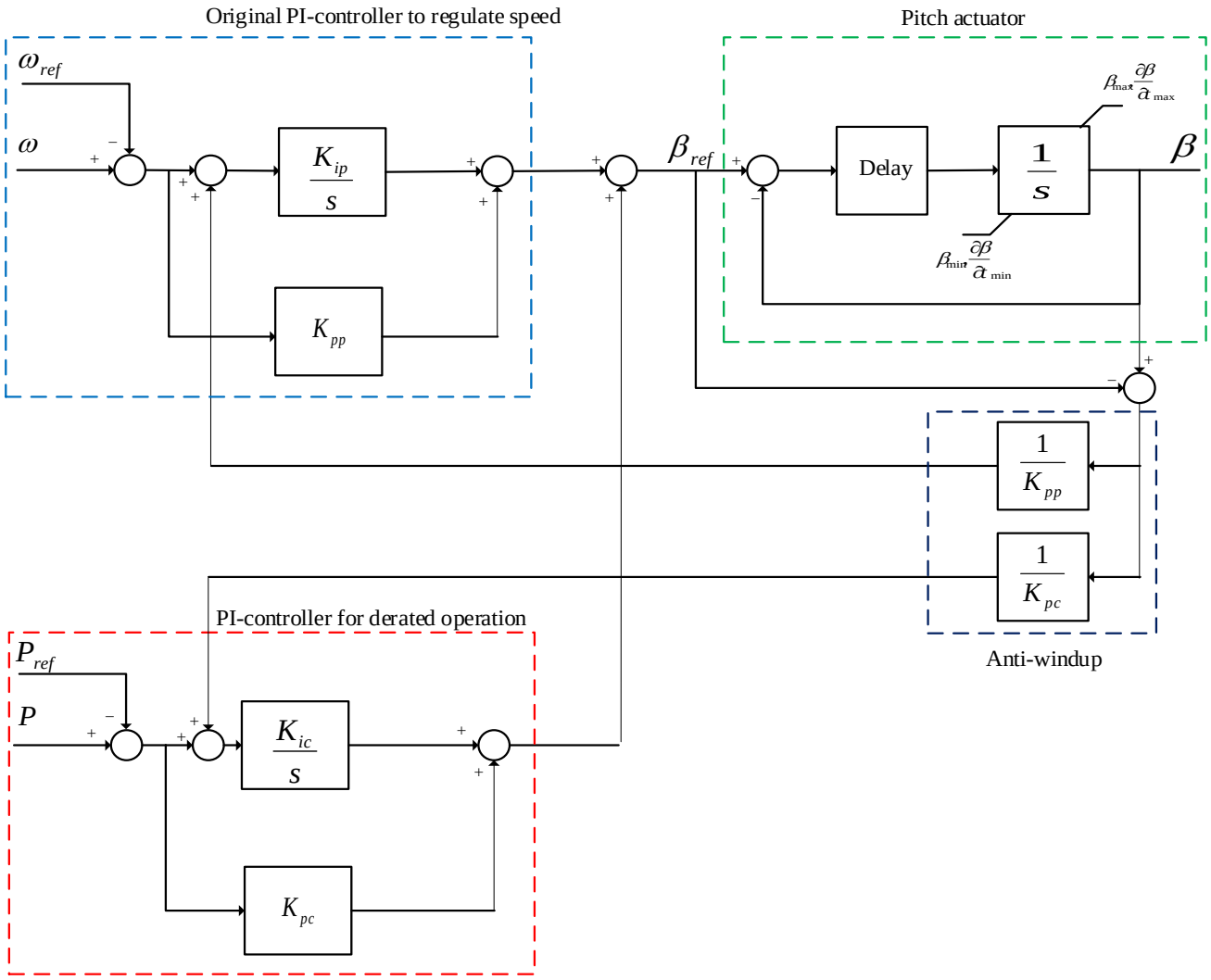

Figure 29: Modified pitch controller. The original pitch controller included the parts inside the blue and green boxes. The added PI-controller for derated operation is shown in the red box and the anti-windup is shown in the black box.

4.3 Implementation of MPPT using Matlab interface

The MPPT is implemented using the built-in Matlab interface in PowerFactory. The latter sends signals to Matlab every time step which then performs a certain action, e.g. running a script or a Simulink simulation, using the signals from PowerFactory. This means that Matlab does not run a simulation in parallel with PowerFactory. Since the MPPT designed in this thesis performs a steady-state calculation, it is enough to use a Matlab script exactly as is done in Chapter 3. The script is essentially the same as the one used in Chapter 3 but has been changed slightly to adapt it to non-ideal wind turbines, see Section 4.3.1. Moreover, the script has been adapted to handle the function call from PowerFactory.

4.3.1 MPPT adaption to non-ideal wind turbines

The DFIG wind turbine model in PowerFactory is non-ideal since it includes losses in the generator. Moreover, the original MPPT did not consider that the power coefficient is also dependent on the operating point of the wind turbine. For example, it is not always possible to have an optimal power coefficient due to operating constraints of the wind turbine, e.g. the maximum turbine speed. The operating constraints are explained in more detail in Section 2.3. Consequently, the original MPPT had to be modified to take into account losses and possible constraints on the power coefficient.

To take the operating constraints into consideration, the turbine power constraint is changed. By using the active power reference and wind speed calculated by the algorithm for the given design variables, the speed reference can be calculated using

$$\omega_{ref} = -0.67P_{ref}^2 + 1.42P_{ref} + 0.511875 \tag{38}$$

where P_{ref} is the active power reference. This expression is used in the DFIG wind turbine controller model to calculate the speed reference based on the actual active power output of the generator. With knowledge of the turbine speed and also the wind speed, the tip-speed ratio can be calculated using (16). Now the maximum power coefficient can be calculated using a look-up table and setting the pitch angle to zero. By using the maximum power coefficient, the maximum possible active power output is calculated using (24). This maximum possible active power output replaces the former limit of the constraint. The new constraint is thus

$$P_i \leq P_{i,max} \tag{39}$$

and ensures that the active power references can actually be fulfilled by the non-ideal wind turbine.

The losses in the wind turbine generator are taken into account by letting the MPPT algorithm perform the optimization on the mechanical side of the generator. This leads to active power references on the mechanical side but since the current regulator in the DFIG wind turbine controller model requires power references on the output side of the generator, the references must be transformed. By assuming a constant efficiency, this transformation can be done as

$$P_{ref} = P_{turb,ref} \cdot \eta \tag{40}$$

where $P_{turb,ref}$ is the active power reference on the mechanical side and η is the efficiency of the generator. Tests in PowerFactory have shown that this assumption is indeed valid.

4.4 Implementation of wake effect model

As stated in Section 4.1.1, the wake effect model is split up into several small models. This is a must in order to fix the initialization of the turbine controller model. The power coefficient, which is the output of the turbine controller model, is used in the wake model to calculate the wind speed of the downstream turbines. This implies that the initialization must start with the first turbine for which the wind speed is known. Once the first turbine has been initialized, its power coefficient is known which means that the wind speed of the second wind turbine can be calculated. This is the same as initializing the first wake model. With the wind speed of the second wind turbine known, initialization can be performed for that specific turbine. Consequently, the initialization has to be performed in a chain, i.e. wind turbine 1 - wake model 1 – wind turbine 2 –wake model 2 and so on.

Each wake model consists of two blocks. The first block contains time delays to represent that it takes time for the wind to travel between the turbines, i.e. if a wind turbine changes its operating state that will be reflected in the wind speed of the downstream turbines after a certain time delay. PowerFactory does however not support variable time delays. Due to this, the delay times are fixed to values which correspond to the delay at the initial wind speed. The second block contains the actual wind speed calculation and is implemented using the Matlab interface, i.e. the actual calculations are performed in Matlab.

5 Verification of the model in DIgSILENT PowerFactory

This chapter includes five simulations performed in PowerFactory with the MPPT implemented. The purpose of the simulations is to verify that it works as intended. The wind farm used in PowerFactory is the same as in the algorithm evaluation and is described in Section 3.3.1. In all simulations, the results are only shown for one row of turbines. The other rows show a more or less identical response and are not shown here in order to save space.

5.1 Wind speed step

Similar to the wind speed step test in the Simulink simulations, a wind speed step is made and the MPPT should respond to this by finding the new optimal operating conditions. Steady-state is also tested here. The initial wind speed is $10\ \mathrm{m/s}$ throughout the whole wind farm. At $t = 5\ \mathrm{s}$, a wind speed step of $1\ \mathrm{m/s}$ brings the incoming wind speed to $11\ \mathrm{m/s}$. The wind direction is orthogonal to the radials, i.e. there are three turbines in each row. The results from the simulation are shown in Figure 30 - Figure 35.

As can be seen in Figure 30, the wind speed is stepped to $11\ \mathrm{m/s}$ at $t = 5\ \mathrm{s}$. Since the first MPPT update occurs at $t = 10\ \mathrm{s}$, the first turbine in the row experiences a higher wind speed but its active power reference is still the same. To fulfill this reference, the added PI-controller in the pitch controller will start to increase the pitch angle to spill the excess wind which can be seen as the highest peak in Figure 32. The increased pitch angle reduces the power coefficient as shown in Figure 33, i.e. wind is spilled. After the MPPT has made its first update, new active power references are sent to the individual turbines, see Figure 31. This will cause the added PI-controller in the pitch controller to reduce the pitch angle, see Figure 32, since the error between actual active power and its reference becomes negative. The reduced pitch angle increases the power coefficient, see Figure 33, which in turn increases the mechanical power input to the turbine, i.e. more wind is captured. With more input of mechanical power than electrical output power, the turbine speed will start to increase, see Figure 34. This increase in speed will cause a speed error in both the pitch controller and the speed controller. The consequence is that the speed controller will increase the electrical output power and the pitch controller will reduce the pitch angle, see Figure 31 and Figure 32 respectively. Due to badly tuned regulators, it takes approximately 100 seconds to reach a new steady-state for the first turbine. It is however considered out of the scope for this thesis to tune the regulators since their performance does not affect the main results. The procedure is repeated for the two following turbines when the wind speed step reaches them as the figures show. Finally, Figure 35 shows how the total wind farm active power output increases as the wind speed step propagates throughout the farm. By careful inspection of Figure 31, it can be seen that the active power output of WT 2 and WT 3 increases slightly after the MPPT update at $t = 10\ \mathrm{s}$ even though the wind speed step has not yet reached those turbines. This increase is possible since the turbines were derated prior to the new references, consequently the active power output can be increased by as much as the turbines were derated.

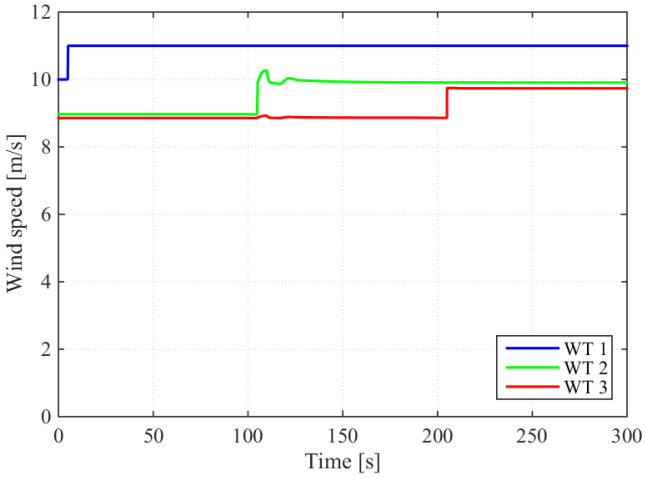

Figure 30: Wind speed of the first row of wind turbines.

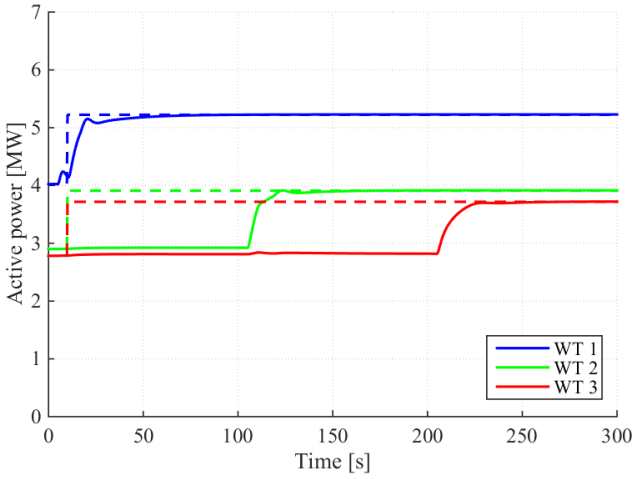

Figure 31: Active power output of the first row of wind turbines, dashed lines are references.

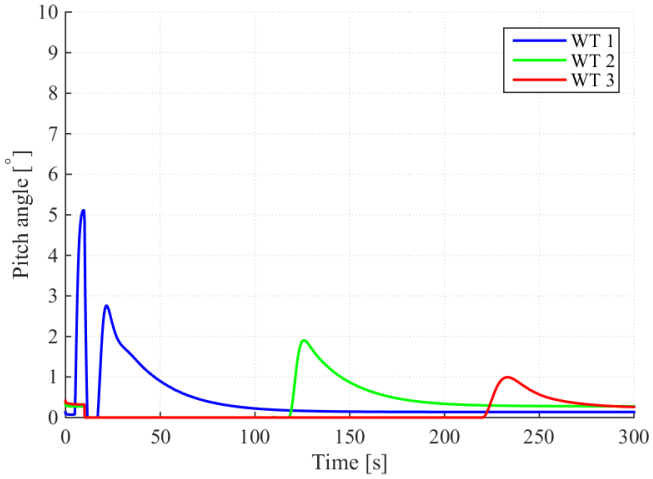

Figure 32: Pitch angles of the first row of wind turbines.

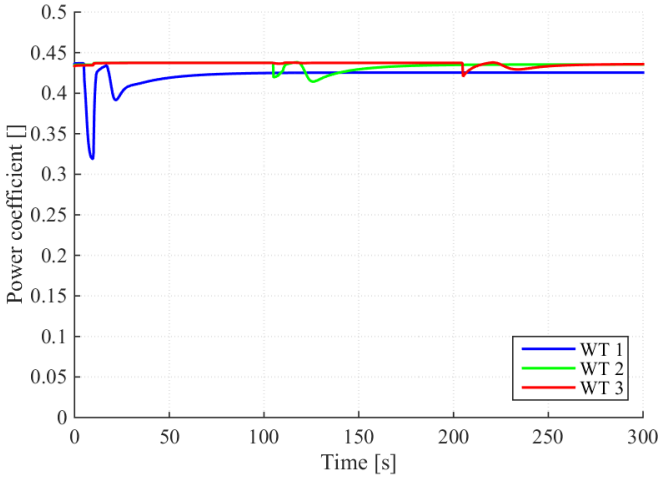

Figure 33: Power coefficients of the first row of wind turbines.

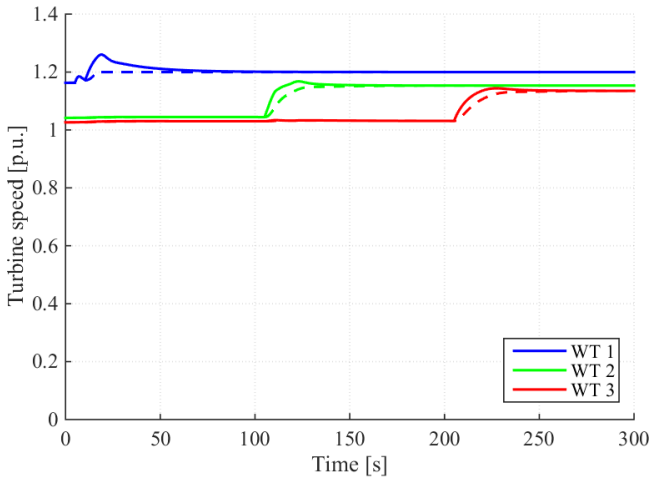

Figure 34: Turbine speed of the first row of wind turbines, dashed lines are references. The speed base is 1.068 rad/s.

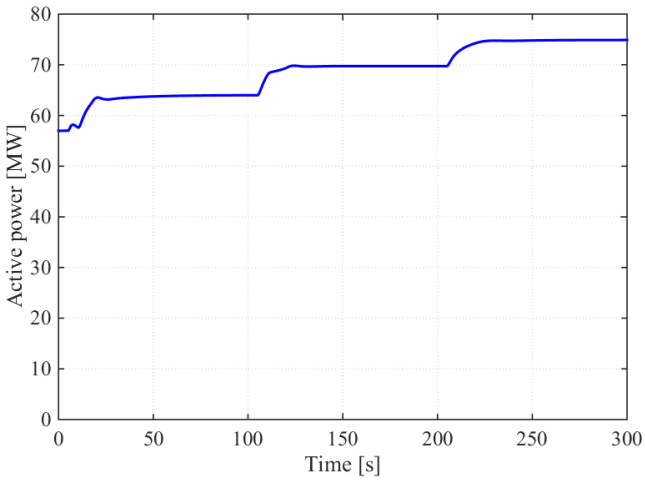

Figure 35: Active power output of the wind farm at PCC.

5.2 Reactive power reference step at PCC

This simulation is very similar to the test made in Simulink, see Section 3.4.3. The purpose is to verify that the MPPT can manage changes in the reactive power reference. Moreover, the simulation also tests that a steady-state is reached. A step is made for the reactive power reference at PCC. The reference is initially 0 MVAr but at $t = 5$ s the reference is stepped to 15 MVAr. Throughout the whole simulation, the incoming wind is at the turbine farthest away from the offshore substation and the wind speed is kept constant at $10\ \mathrm{m/s}$. The results are shown in Figure 36 - Figure 39.

As Figure 36 shows, the reactive power reference is stepped at $t = 5$ s but the output remains constant until $t = 10$ s. This is because the first MPPT after the reference step occurs at $t = 10$ s. Once the MPPT has updated and sent new references to the individual turbines the output changes. This increase in reactive power output is very smooth and settles close to the reference. The final value will not necessarily be equal to the reference due to the non-linear constraint, see Section 3.1.7. Figure 37 - Figure 39 indicate that the wind farm is able to change its reactive power output without affecting the active power output and turbine speed.

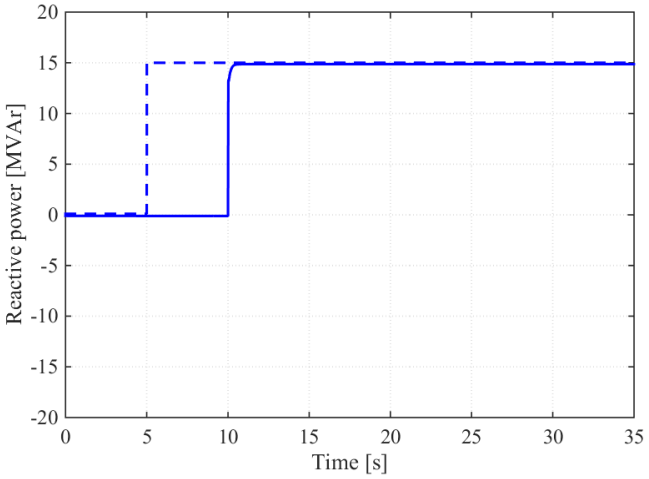

Figure 36: Reactive power output of the wind farm at PCC, the dashed line is the reference.

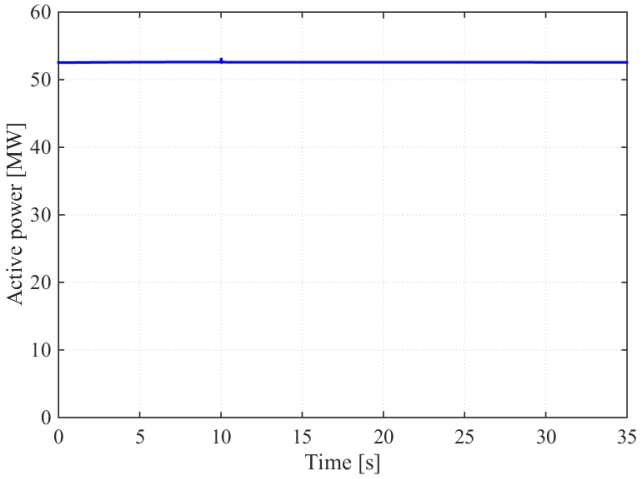

Figure 37: Active power output of the wind farm at PCC.

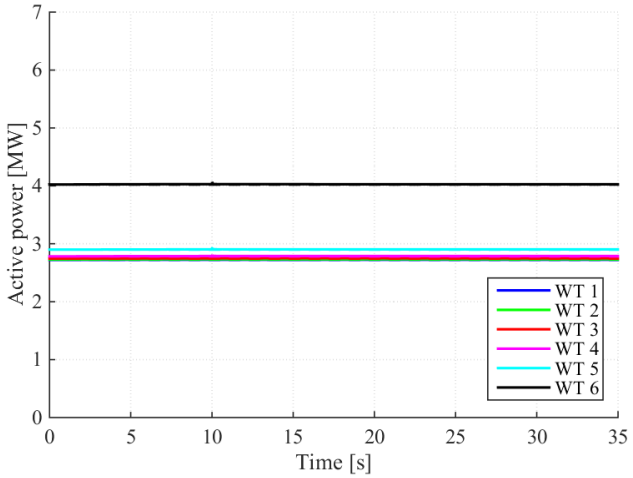

Figure 38: Active power output of the first row of wind turbines.

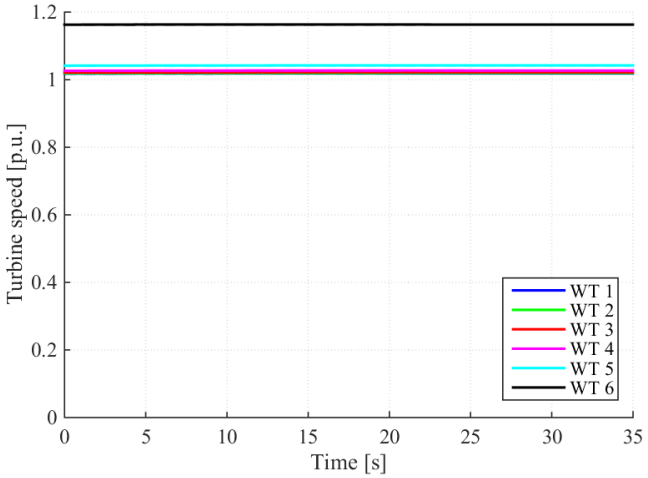

Figure 39: Turbine speed of the first row of wind turbines, the speed base is 1.068 rad/s.

5.3 Reactive power reference ramp at PCC

This simulation is an extension of the reactive power reference step simulation in Section 5.2. Instead of applying a step to the reactive power reference at PCC, a ramp increase is used. The initial reference is 0 MVAr, at $t = 1$ s the ramp starts with a slope of 0.5 MVAr per second. Two cases are studied, capacitive and inductive output which corresponds to positive and negative slope respectively. The reference is kept increasing throughout the whole simulation in order to verify that the MPPT can handle a situation where the reactive power reference is higher than what the farm can output. In both cases, the wind direction is orthogonal to the radials and the incoming wind speed is kept constant at 10 m/s.

5.3.1 Capacitive output

This case considers positive reactive power output of the wind farm, i.e. capacitive operation and the results from the simulation can be seen in Figure 40 - Figure 42. . The reactive power output curve of the wind farm is stair step shaped as shown in Figure 40. The shape is a result of the MPPT update frequency which is set to 10 seconds. Consequently, when the MPPT updates it will use the reference at that time instant. In between each updates the output is constant, thus resulting in a stair step shaped curve. The last MPPT update is made at $t = 50$ s. As can be seen, the step made is not enough to reach the reference at $t = 50$ s. This is due to that the maximum reactive power output limit (capacitive) of the wind farm is reached. As Figure 42 shows, the bus voltage limits has been reached thus limiting the reactive power output of the wind farm. Figure 41 shows the active power output of the wind farm. It remains more or less constant throughout the whole simulation even though the reactive power output changes.

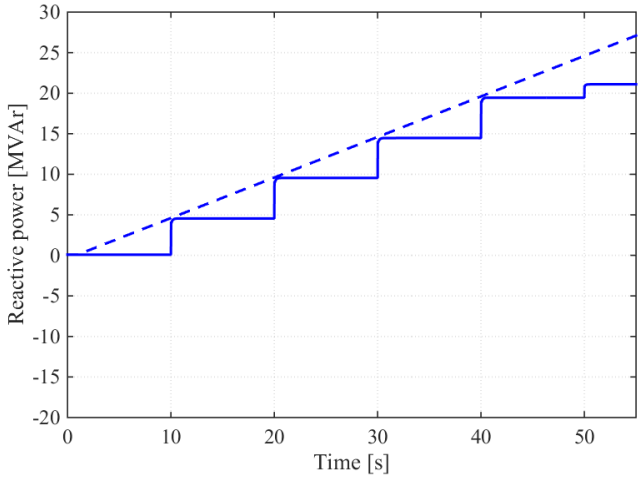

Figure 40: Reactive power output of wind farm, the dashed line is the reference.

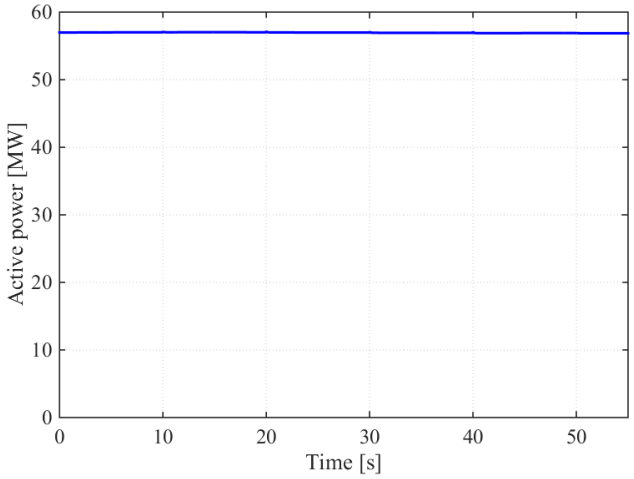

Figure 41: Active power output of wind farm.

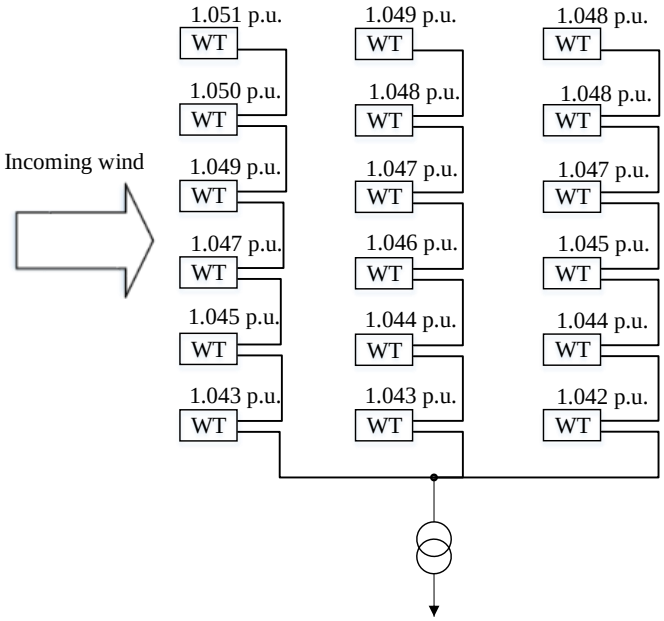

Figure 42: Bus voltages at maximum capacitive operation.

5.3.2 Inductive output

This case considers negative reactive power output of the wind farm, i.e. inductive operation, and the results from the simulation can be seen in Figure 43 - Figure 45. At the end of the simulation, from the MPPT update at $t = 100$ s and onwards, the reactive power output remains constant even though a MPPT update is made at $t = 110$ s. The simple reason for this is that the reactive power output limit of the wind farm is reached since the wind turbines have reached their maximum inductive operating point. The bus voltages are well within the allowed limits, see Figure 45. Figure 44 shows the active power output of the wind farm. It can be seen that the active power output drops slightly during the simulation; this is mainly because of the approximate way in which the reactive power limits of the wind farm is calculated, see Section 3.1.7.

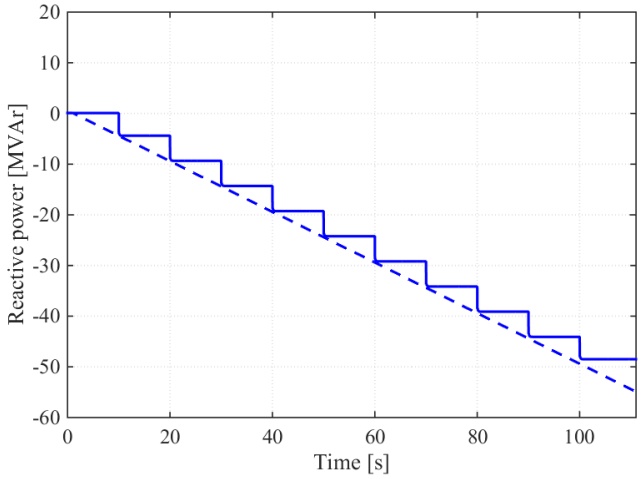

Figure 43: Reactive power output of wind farm, the dashed line is the reference.

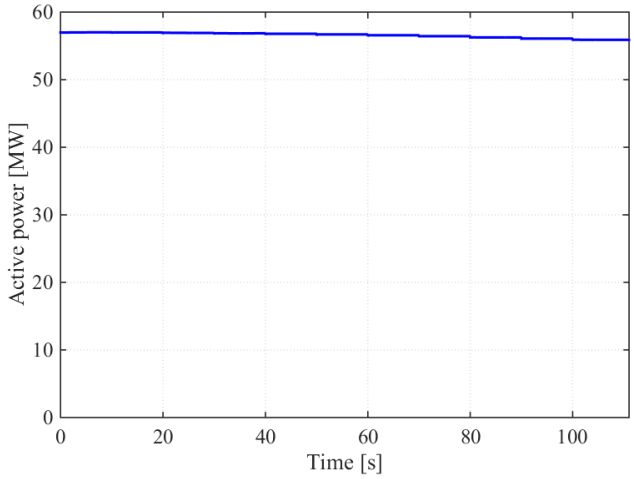

Figure 44: Active power output of wind farm.

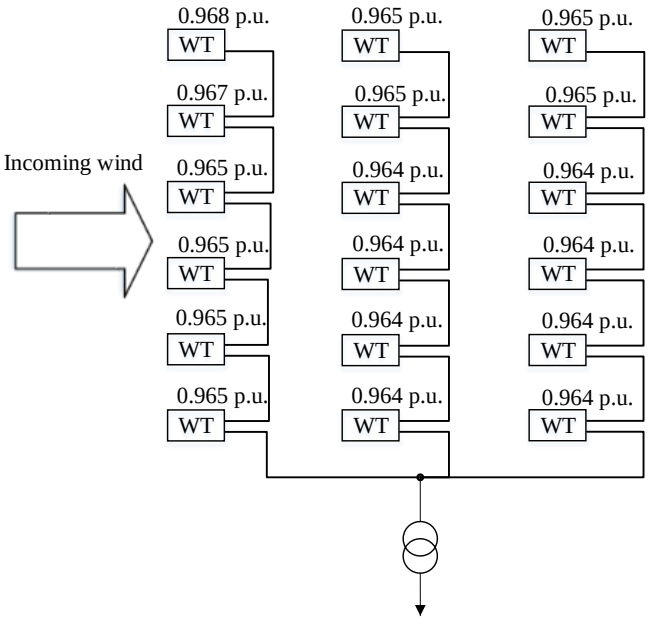

Figure 45: Bus voltages at maximum inductive operation, i.e. at the end of the simulation.

5.4 LVRT simulation

The purpose of this test is to ensure that the wind turbines are still capable of their normal LVRT even though they are receiving references from the MPPT. In other words, the wind turbines should behave as usual during a voltage dip. This test is done by reducing the voltage at PCC to simulate a severe disturbance in the grid, e.g. a three-phase short-circuit. At $t = 5$ s, the voltage at PCC is reduced to 0.2 p.u. for 0.5 s and then returns to 1.0 p.u. at $t = 5.5$ s. Throughout the whole simulation, the incoming wind is at the turbine closest to the offshore substation and the wind speed is kept constant at $10\ \mathrm{m/s}$. The results from the simulation are shown in Figure 46 - Figure 51.

When the voltage at PCC falls at $t = 5$ s, see Figure 46, the voltage also falls at the turbine terminals, see Figure 47. Because of the low voltage, the turbines cannot deliver as much power to the grid as before which causes the active power output of the turbines to fall, see Figure 48. As a consequence of this, the turbine speed will start to increase, see Figure 49, since the input mechanical power exceeds the electrical output power. When the voltage at PCC returns to 1.0 p.u. at $t = 5.5$ s, the electrical output power can increase again. Since the turbine speed deviates from its reference, the speed controller will respond to this by increasing the electrical output power. This can be seen as the overshoots in Figure 48. Finally, the speed approaches its reference together with the electrical output power.

The built-in wind turbine controller model in PowerFactory has a protection system which may perform different actions in a low voltage situation. If the voltage drops below a certain pre-set value and remains below that value for a pre-set time, the wind turbine will automatically disconnect. In the same way, the wind turbine can disconnect if the turbine speed exceeds a certain pre-set value and remains above that value for a pre-set time.

Moreover, when the voltage is outside a certain dead band centered around the nominal value, the reactive power support is activated in order to increase the voltage. In this simulation, the voltage drop is such that reactive power support will be activated but the dip is too short to cause tripping. Moreover, the turbine speed is below the tripping value. Figure 50 shows that the reactive power output of the wind turbines increases to approximately 2 MVAr during the dip. The output cannot go higher since the rotor current limit is reached. Figure 51 shows the total reactive power output of the wind farm. Note the spikes in Figure 50 and Figure 51 that occur when the voltage dip begins and ends respectively. The stator voltage is closely related to the stator flux in the induction machine. Consequently, when the voltage abruptly changes value there will be a change in the exchange of reactive power between the machine and the grid. This can be seen as the spikes in Figure 50 and Figure 51.

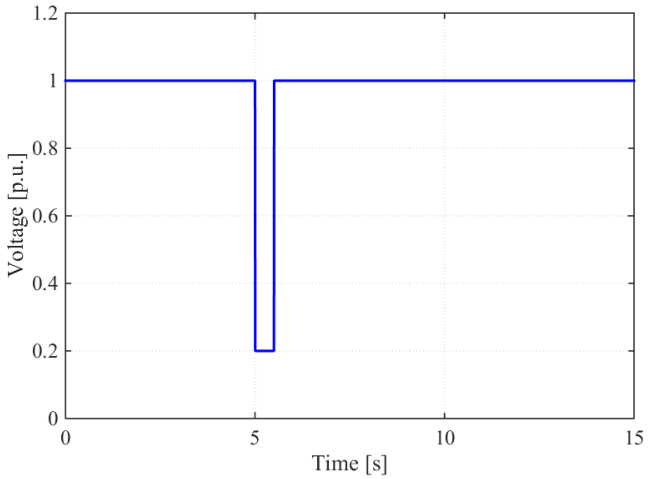

Figure 46: Bus voltage at PCC, the voltage base is 132 kV.

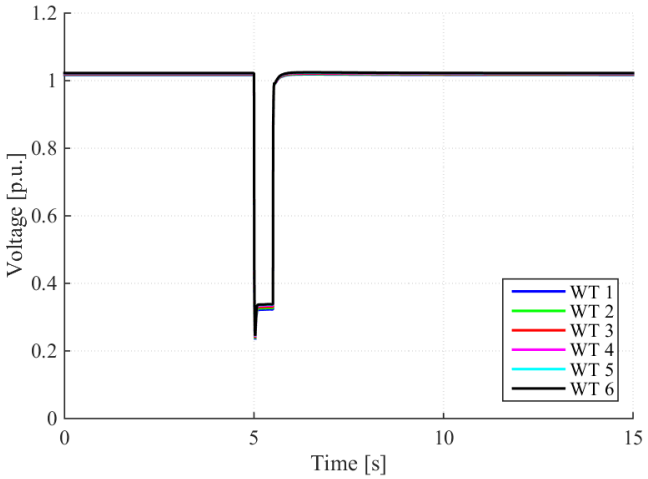

Figure 47: Turbine bus voltages, the voltage base is 0.69 kV.

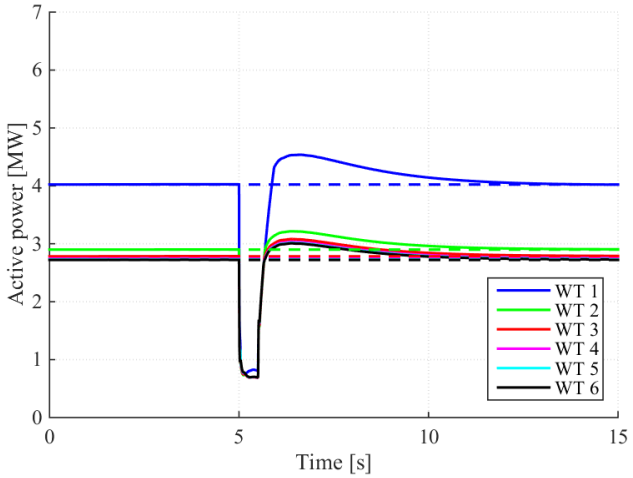

Figure 48: Active power output of the first row of wind turbines, dashed lines are references.

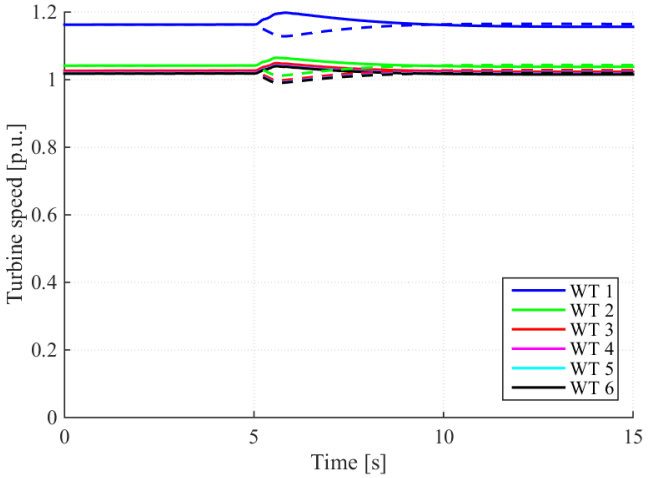

Figure 49: Turbine speed of the first row of wind turbines, dashed lines are the references. The speed base is 1.068 rad/s.

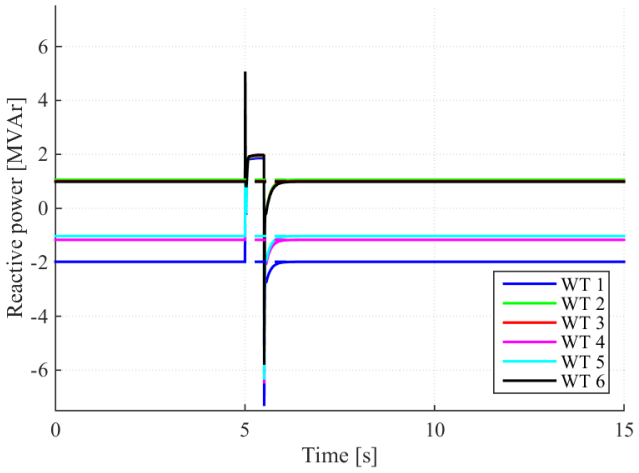

Figure 50: Reactive power output of the first row of wind turbines, dashed lines are references.

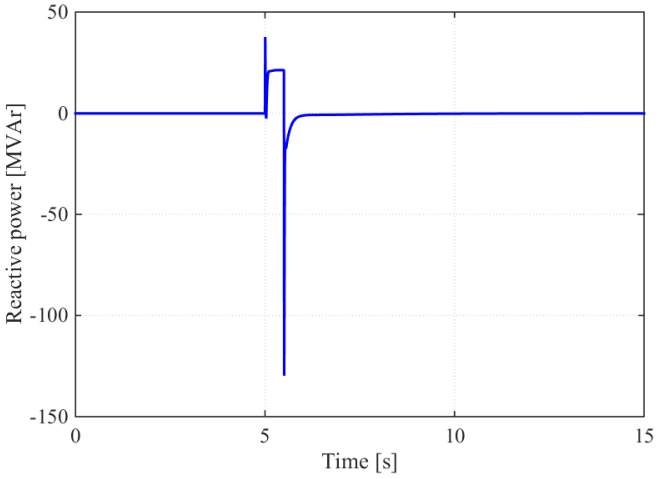

Figure 51: Reactive power output of the wind farm at PCC.

5.5 Disconnection of one radial

In this simulation, one radial is manually tripped in order to verify that the MPPT can handle it, i.e. the MPPT should be able to maximize the active power output even if one or more wind turbines and/or radials are out of service. The wind direction is orthogonal to the radials and the wind speed is kept constant at $t = 10\ \mathrm{m/s}$ throughout the whole simulation. At $t = 5$ s, the most upwind radial trips thus disconnecting six wind turbines from the wind farm.

The results from the simulation are shown in Figure 52 - Figure 57. As shown in Figure 52 when the radial trips the output power of the WT1, which is situated on the tripped radial, goes to zero. However, since the MPPT has not yet been updated the power references remain the same. Figure 53 shows that when the radial trips, the output active power of the wind farm drops to almost half of its original value. The drop is this significant since it was the most upwind radial that tripped. At $t = 10$ s, the MPPT is updated and new power references are sent to the turbines as seen in Figure 52. However, the wind speeds required to reach these new references have not yet reached WT2 and WT3, as can be seen in Figure 54. At $t = 105$ s and $t = 205$ s respectively, the higher wind speed reaches WT2 and WT3 which can then reach their power references, see Figure 52. The pitch angles are shown in Figure 55 and as can be seen, once WT1 trips the pitch angle will be increased in order to stop the wind turbine. This is reflected in the power coefficient, see Figure 56. Note that the negative power coefficient of WT1 is non-realistic and caused by negative data in the $C_p(\lambda, \beta)$ lookup table. The final plot in Figure 57 shows the turbine speeds. Even though disconnected, WT1 settles at a non-zero speed. This is due to how the built-in model's shut down process is designed and is unimportant in this case.

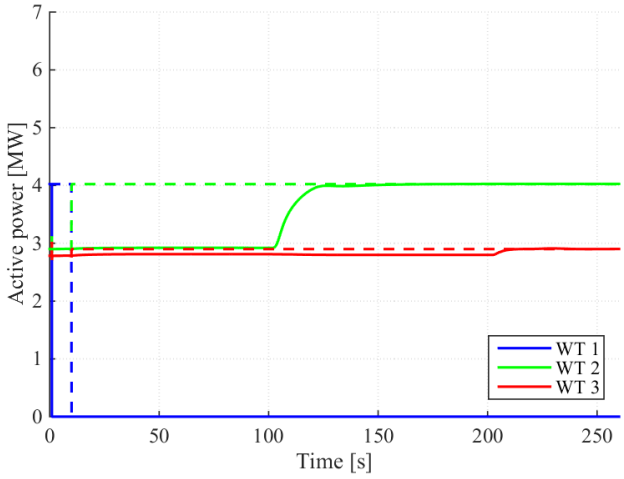

Figure 52: Active power output of the first row of wind turbines, dashed lines are references.

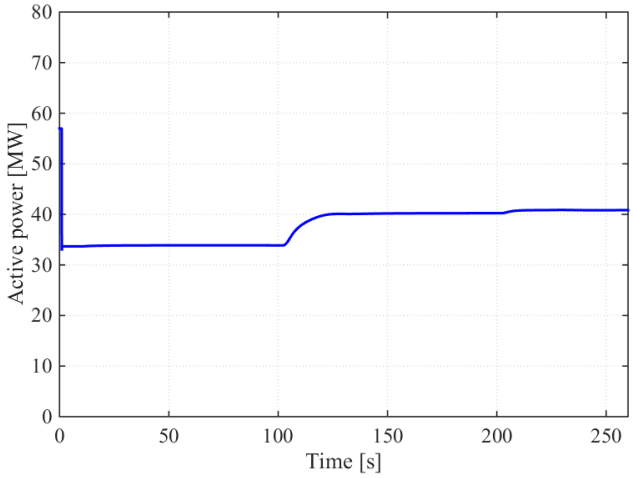

Figure 53: Active power output of the wind farm at PCC.

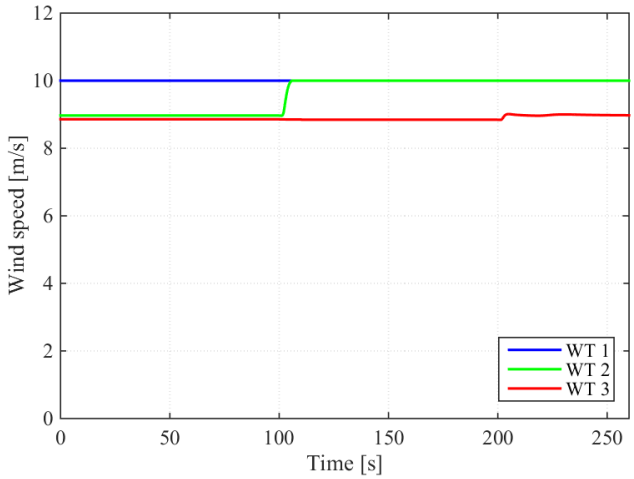

Figure 54: Wind speed of the first row of wind turbines.

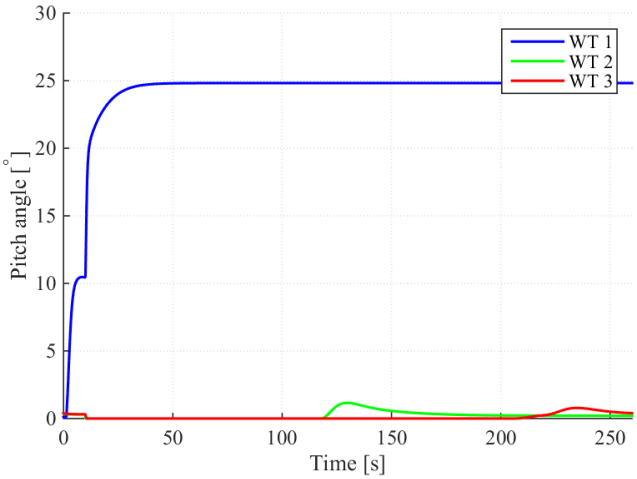

Figure 55: Pitch angles of the first row of wind turbines.

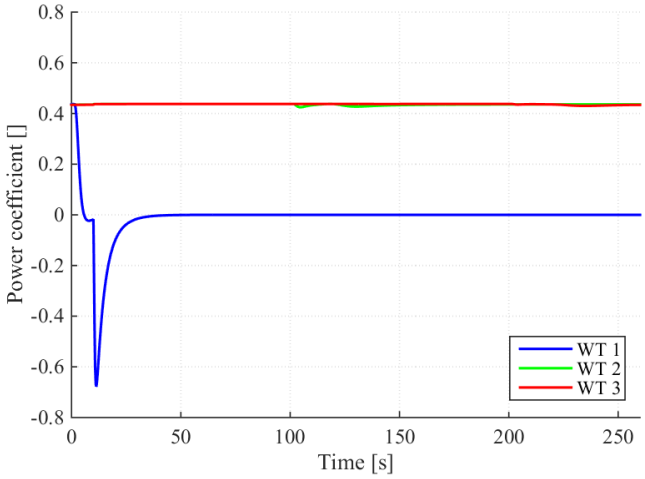

Figure 56: Power coefficients of the first row of wind turbines.

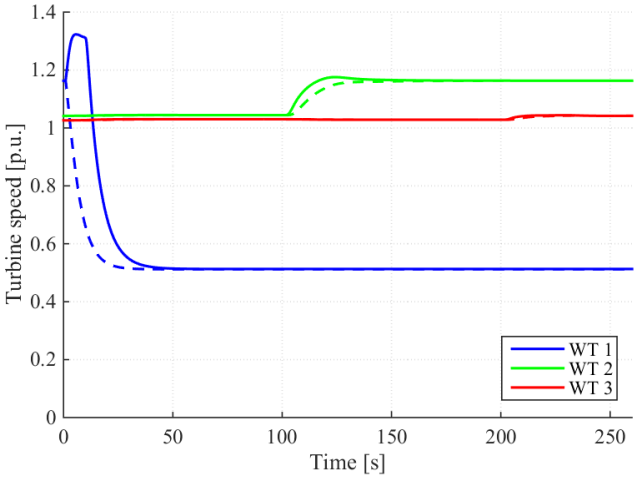

Figure 57: Turbine speed of the first row of wind turbines, dashed lines are references. The speed base is 1.068 rad/s.

6 Discussion

The results in this thesis show that it is important to consider the wake effect when it comes to wind farm control. By utilizing some form of coordinated control, e.g. like the approach used in this thesis, the power harnessed by the wind farm can be increased by a few percent. However, different approaches have different requirements for them to function properly. The approach developed in this thesis is based on steady-state calculations of the optimal operating points of the individual turbines in the wind farm. Since the incoming wind is constantly changing, this steady-state calculation is ideally performed as often as possible. However, it takes time to perform the optimization so there is a limit on how often it can take place. For the approach used in this thesis to be practically useful, the speed of the optimization algorithm has to be increased. One way of increasing the speed of the algorithm is to use another kind of load flow calculation method. Instead of using Newton-Raphson to solve the power flow equations, the so-called Backward/Forward power flow method could be used. This method is especially fast when it comes to radial systems. This applies to the wind farm since it is indeed a radial system. It is thus possible that the Backward/Forward power flow method could increase the speed of the algorithm. Elaborating further on the speed issue, tests have shown that the computer used strongly affects the time required to perform the optimization. For example, the time needed to perform one optimization calculation is reduced from 55 seconds to 19 seconds only by changing the computer. The conclusion from this test is that in a real-life application, the choice of hardware has to be made very carefully to ensure the highest possible performance.

As compared to the previous work done in the field of coordinated wind farm control, the approach used in this thesis also takes into account the losses in the collector system when performing the optimization. The results indicate that the gain from also considering the losses is comparably small and depending on the situation even negligible. However, there is no clear evidence from the algorithm evaluation that it takes less time to perform the optimization without taking the collector system losses into account. Consequently, the collector system losses might as well be included.

The MPPT designed in this thesis requires that the incoming wind speed is known which implies that it has to be measured. There are basically two ways of accurately measuring the incoming wind speed, either via a measuring mast or through the use of LIDAR, which is a laser based measurement technology. In existing wind farms today, the incoming wind speed is not always measured which poses a problem when implementing the MPPT in this thesis. It is therefore important to be aware of the fact that some kind of measurement equipment might have to be installed in case this MPPT is to be implemented.

One of the goals of the thesis is to design a generic MPPT, i.e. the model should be applicable to wind turbines from different manufacturers as well as different wind farm layouts. The only turbine specific input data in the optimization algorithm is the rotor diameter, the so-called turbine constant ($0.5\rho A^2$), the PQ-curve and the power coefficient curve. The rotor diameter and the turbine constant are easily obtained for any turbine while the power coefficient curve can be harder to find. In case the power coefficient curve cannot be obtained for a specific

turbine, a generic curve can be used. So consequently, the first requirement is fulfilled. The MPPT algorithm is written in a way that requires the wind turbines to be placed in rows with a variable separation distance. However, if several rows are wanted they must be identical to the first row. This puts some restrictions on the wind farm layout but makes the MPPT algorithm simpler and faster. Consequently, the MPPT can be considered as fairly generic.

The existing MPPT is basically only for steady-state operation and all dynamics are put on the wind turbines themselves. However, at present the power references are still sent to the wind turbines. A smarter way might be to change strategy during abnormal operating conditions, e.g. under/over frequency and under/over voltage. By having frequency as an input would create an interesting possibility to include frequency regulation capabilities in the MPPT in case of under/over frequency. An example of this is inertia response, i.e. to use the stored kinetic energy in the rotating mass to decrease the rate of change of frequency (ROCOF) during a grid disturbance. By having for example the PCC bus voltage as input, a voltage dip could be detected by the MPPT which can then respond in a proper way by sending new power references. The strategies for abnormal operating conditions must be decoupled from the ordinary update frequency of the MPPT since they have to be more or less instant. It is worth noting that by including strategies for abnormal operating conditions, the MPPT is turned into a wind farm controller which is not the original aim of the thesis.

7 Conclusions

Coordinated control of wind turbines in wind farms is important in order to increase the active power output, especially in large wind farms where the wake effect is more prominent. By proper control, the total active power output of a wind farm can be increased by more than one percent. The MPPT developed in this thesis takes into account both the wake effect and collector system losses when performing the optimization. Moreover, it also considers reactive power dispatch, cable current capability and bus voltage limits.

An evaluation of the algorithm shows that the active power output of a sample wind farm consisting of 18 wind turbines, each rated 6 MW, can increase with as much as 1.30 % as compared to the normal strategy of performing MPPT operation individually at each wind turbine. The corresponding increase by considering the wake effect only is 1.27 %. At the same time, the losses are decreased by up to 1 % as compared to only considering the wake effect. An important issue to consider is the speed of the algorithm. The MPPT developed in this thesis is too slow for real applications so it has to be improved. A way of speeding up the algorithm could be to use the Backward/forward power flow method.

The MPPT has also been successfully implemented in DIgSILENT PowerFactory. It is ready to be used for dynamical power system simulations as well as load flow calculations.

7.1 Future work

As stated in the discussion and conclusions, an important aspect of the MPPT is the time needed to perform an optimization and that the current version is too slow for real applications. As a first try to improve the speed of the MPPT, the Backward/Forward load flow should be implemented and tested.

When for example a wind speed step occurs at the first wind turbine in a row, the MPPT will recalculate the power references for all wind turbines and update them. However, the downstream wind turbines will not yet experience the new wind speed since it takes time for the wind speed step to propagate throughout the wind farm. This leads to a sub-optimal operating point for the whole wind farm until the wind speed step has reached the end turbine of the row. One way of improving the MPPT would be to evaluate when the power references should be updated to avoid this sub-optimal condition.

As stated in the discussions chapter, strategies for abnormal operating conditions could be implemented, e.g. frequency and voltage regulation capabilities. This would turn the MPPT into a sort of wind farm controller which would be more complete and suitable for real applications.

References

[1] T. Burton, N. Jenkins, D. Sharpe and E. Bossanyi, Wind Energy Handbook, Chichester: John Wiley & Sons Ltd, 2011.

[2] G. Tarnowski, P. Kjær, S. Dalsgaard and A. Nyborg, "Regulation and frequency response service capability of modern wind power plants," in *Power and Energy Society General Meeting, 2010 IEEE*, 2010.

[3] E. Bitar and P. Seiler, "Coordinated Control of a Wind Turbine Array for Power Maximization," in *American Control Conference*, 2013.

[4] J. Shu, B. Zhang and Z. Bo, "A wind farm coordinated controller for power optimization," in *Power and Energy Society General Meeting*, 2011.

[5] K. Johnson and T. Navee, "Wind Farm Control: Addressing the Aerodynamic Interaction Among Wind Turbines," in *American Control Conference*, 2009.

[6] F. van Dam, P. Gebraad and J. van Wingerden, "A maximum power point tracking approach for wind farm control," Delft Center for Systems and Control, Delft University of Technology, 2012.

[7] H. Bahirat, B. Mork and H. Hoidalen, "Comparison of Wind Farm Topologies for Offshore Applications," in *IEEE Power and Energy Society General Meeting*, 2012.

[8] B. Singh and S. N. Singh, "Reactive Capability Limitations of Doubly-fed Induction Generators," *Electric Power Components and Systems*, pp. 427-440, 2009.

[9] J. Dahlberg, "Lillgrund Pilot Project," Vattenfall Vindkraft AB, 2009.

[10] N. Jensen, "A Note On Wind Generator Interaction," Risö, 1983.

[11] J. Arora, Introduction to Optimum Design, San Diego: Elsevier Academic Press, 2004.

[12] H. Saadat, Power System Analysis, PSA Publishing, 2010.

[13] T. Thiringer, J. Paixao and M. Bongiorno, "Monitoring of Ride-Through Ability of a 2 MW Wind Turbine in Tvååker, Halland," Elforsk, 2009.

[14] T. Sörensen, M. Thögersen and P. Nielsen, "Adapting and Calibration of Existing Wake Models to Meet the Conditions Inside Offshore Wind Farms," EMD International, Ålborg, 2008.

[15] N. D. GmbH, *Submarine Power Cables - Datasheet*, Hannover, 2013.

[16] J. Andersson, C. Karlsson and Q. Wang, "Inertia Support from Pitch-regulated, Full Power Converter Wind Turbines," Gothenburg, 2014.

[17] K. Clark, N. Miller and J. Sanchez-Gasca, "Modeling of GE Wind Turbine Generators for Grid Studies," General Electric, 2008.

[18] I. Katic, J. Hojstrup and N. Jensen, "A Simple Model for Cluster Efficiency," in *European Wind Energy Association*, Rome, 1986.